40390

National Library of Canada | Bibliothèque nationale du Canada

CANADIAN THESES ON MICROFICHE | THÈSES CANADIENNES SUR MICROFICHE

NAME OF AUTHOR/*NOM DE L'AUTEUR* Couch, Janet Struthers

TITLE OF THESIS/*TITRE DE LA THÈSE* A Spectrographic Study of DE Draconis: The Orbit and Rotation Effect

UNIVERSITY/*UNIVERSITÉ* University of Alberta

DEGREE FOR WHICH THESIS WAS PRESENTED/*GRADE POUR LEQUEL CETTE THÈSE FUT PRÉSENTÉE* M.Sc.

YEAR THIS DEGREE CONFERRED/*ANNÉE D'OBTENTION DE CE GRADE* 1979

NAME OF SUPERVISOR/*NOM DU DIRECTEUR DE THÈSE* Dr. D. P. Hube

Permission is hereby granted to the NATIONAL LIBRARY OF CANADA to microfilm this thesis and to lend or sell copies of the film.

The author reserves other publication rights, and neither the thesis nor extensive extracts from it may be printed or otherwise reproduced without the author's written permission.

L'autorisation est, par la présente, accordée à la BIBLIOTHÈQUE NATIONALE DU CANADA de microfilmer cette thèse et de prêter ou de vendre des exemplaires du film.

L'auteur se réserve les autres droits de publication; ni la thèse ni de longs extraits de celle-ci ne doivent être imprimés ou autrement reproduits sans l'autorisation écrite de l'auteur.

DATED/*DATÉ* 3 May 1979 SIGNED/*SIGNÉ* Janet S. Couch

PERMANENT ADDRESS/*RÉSIDENCE FIXÉ* 41 Highpark Crescent
Ottawa Ontario
K1B 3G9

NL-91 (3-74)

National Library of Canada

Cataloguing Branch
Canadian Theses Division

Ottawa, Canada
K1A 0N4

Bibliothèque nationale du Canada

Direction du catalogage
Division des thèses canadiennes

NOTICE

The quality of this microfiche is heavily dependent upon the quality of the original thesis submitted for microfilming. Every effort has been made to ensure the highest quality of reproduction possible.

If pages are missing, contact the university which granted the degree.

Some pages may have indistinct print especially if the original pages were typed with a poor typewriter ribbon or if the university sent us a poor photocopy.

Previously copyrighted materials (journal articles, published tests, etc.) are not filmed.

Reproduction in full or in part of this film is governed by the Canadian Copyright Act, R.S.C. 1970, c. C-30. Please read the authorization forms which accompany this thesis.

THIS DISSERTATION
HAS BEEN MICROFILMED
EXACTLY AS RECEIVED

AVIS

La qualité de cette microfiche dépend grandement de la qualité de la thèse soumise au microfilmage. Nous avons tout fait pour assurer une qualité supérieure de reproduction.

S'il manque des pages, veuillez communiquer avec l'université qui a conféré le grade.

La qualité d'impression de certaines pages peut laisser à désirer, surtout si les pages originales ont été dactylographiées à l'aide d'un ruban usé ou si l'université nous a fait parvenir une photocopie de mauvaise qualité.

Les documents qui font déjà l'objet d'un droit d'auteur (articles de revue, examens publiés, etc.) ne sont pas microfilmés.

La reproduction, même partielle, de ce microfilm est soumise à la Loi canadienne sur le droit d'auteur, SRC 1970, c. C-30. Veuillez prendre connaissance des formules d'autorisation qui accompagnent cette thèse.

LA THÈSE A ÉTÉ
MICROFILMÉE TELLE QUE
NOUS L'AVONS REÇUE

THE UNIVERSITY OF ALBERTA

A SPECTROGRAPHIC STUDY OF DE DRACONIS: THE ORBIT AND ROTATION EFFECT

by

© JANET STRUTHERS COUCH

A THESIS

SUBMITTED TO THE FACULTY OF GRADUATE STUDIES AND RESEARCH

IN PARTIAL FULFILMENT OF THE REQUIREMENTS FOR THE DEGREE

OF MASTER OF SCIENCE

DEPARTMENT OF PHYSICS

EDMONTON, ALBERTA

SPRING, 1979

THE UNIVERSITY OF ALBERTA

FACULTY OF GRADUATE STUDIES AND RESEARCH

The undersigned certify that they have read, and recommend to the Faculty of Graduate Studies and Research, for acceptance, a thesis entitled A SPECTROGRAPHIC STUDY OF DE DRACONIS: THE ORBIT AND ROTATION EFFECT submitted by Janet Struthers Couch in partial fulfilment of the requirements for the degree of Master of Science.

.....
Supervisor

.....

.....

.....

.....
External Examiner

Date..29.March.1979.....

ABSTRACT

The eclipsing spectroscopic binary system DE Draconis is re-examined, using 86 new observations obtained between 1976 and 1978 on the 1.8m telescope at the Dominion Astrophysical Observatory in Victoria and one new point from the David Dunlap Observatory in Toronto, together with 18 older data from the DDO in Toronto. The 52 observations outside eclipse allow a more reliable determination of the orbital elements to be made, using the Lehmann-Filhés method of solution, and this allows a velocity curve for the primary to be drawn. The spectrographic results are combined with some previously published photometric and four-colour results to give an approximate picture of the physical parameters of this system.

The very detailed spectrographic study of the velocity changes of the primary star on 53 plates taken during eclipse clearly shows the existence of a rotation effect in the primary's velocity curve. This is analysed using two methods, by Petrie and Hosokawa. The rotational velocity of the primary star, spectral type B9V, is found to be about 180 km/s, indicating that the star does not rotate in synchronism with the system. All results support the previous conclusion that the secondary, although not directly observed, is a main sequence G-type star with normal characteristics.

ACKNOWLEDGEMENTS

I would like to express my deep appreciation to my supervisor, Dr. D.P. Hube, for his continued support, encouragement, and advice throughout my program, and for his care in reading and correcting my thesis. I am also indebted to him for providing the observational data on which this study is based, and for his financial assistance.

I wish to thank the other members, students and staff, of the Astrophysics Section for their help in various areas of my studies. Finally, I express my profound gratitude to my parents for their unfailing understanding and belief in me.

Financial assistance from the National Research Council of Canada, the Province of Alberta, and the University of Alberta is also gratefully acknowledged.

TABLE OF CONTENTS

CHAPTER		PAGE
I.	INTRODUCTION	1
	Historical Recognition of Binary Stars	1
	Classification of Binary Stars	3
	Orbital Elements	5
	Determination and Significance of Orbital Elements	8
	Selection Effects	13
	Velocity Curve Distortion: The Rotation Effect	16
	Previous Work on the Rotation Effect	18
II.	OBSERVATIONAL TECHNIQUES	20
	Some Basic Theory	20
	The Spectrograph	21
	Stellar Spectrograms	23
	Radial Velocity Calculations	23
	Standard Wavelengths	25
III.	THE SPECTROGRAPHIC ORBIT OF DE DRACONIS	29
	Period Determination	29
	Determination of Other Orbital Elements	31
	Previous Orbital Elements of DE Draconis	34
	New Observations	37
	New Orbital Elements	38
	Photometric Data and Physical Parameters	44

IV. THE ROTATION EFFECT 52

General Information 52

Preliminary Theory 57

Petrie's Analysis 58

Hosokawa-Kopal Analysis 66

General Theory 66

Calculations of α-Functions for DE Draconis 74

The Final Formula 79

Comments 81

V. CONCLUDING REMARKS 85

***

SELECTED BIBLIOGRAPHY 92

APPENDIX A. OBSERVATIONAL DATA 96

APPENDIX B. CALCULATIONS OF PHYSICAL PARAMETERS 101

LIST OF TABLES

Table	Description	Page
1.	The Orbital Elements	36
2.	Photometric Elements	37
3.	Final Orbital Elements	39
4.	Fractional Light from the Secondary	46
5.	Physical Parameters of DE Draconis	51
6.	Rotational Velocity Data: Petrie	62
7.	Rotation Effect: Hosokawa	80

LIST OF FIGURES

Figure		Page
1.	Orbital Elements	7
2.	Schematic Diagram of a Spectrograph	22
3.	Final Velocity Curve	42
4.	Observed Velocities Within Eclipse	43
5.	The Configuration for a Transit	54
6.	Projected Disc	57
7.	Projected Configuration of Eclipse	59
8.	Configurations for Petrie's Three Cases	61
9.	Calculated Rotation Curves: Petrie	65
10.	Configuration and Notations for Hosokawa's Analysis	68
11.	Limits for Eclipse Integrals	69
12.	Eclipse Data Points	75
13.	Normal (Averaged) Points from Eclipse Data	77
14.	Calculated Rotation Curves: Hosokawa	83

CHAPTER I

INTRODUCTION

Historical Recognition of Binary Stars

The term 'binary star' was first used by W. Herschel in 1802 to describe "... a real double star--the union of two stars, that are formed together in one system, by the laws of [gravitational] attraction ..." (Herschel 1802). However, the term 'double star' had been used much earlier, by Ptolemy in describing ν Sagitarii--two fifth magnitude stars with an angular separation of about 14 minutes of arc (somewhat less than half the apparent diameter of the moon).

Thus not all 'double stars' are binary systems. The first binary, discovered in 1650, was ζ Ursae Majoris (Mizar). It was also the first double star to be observed photographically, in 1857, and its principal component was the first spectroscopic binary to be identified, in 1889. Algol (β Persei) became the second known spectroscopic binary and the first of the eclipsing binaries, when its spectrum was investigated because of the periodic loss of light observed by Goodricke (1783).

The earliest discoveries made in the seventeenth and most of the eighteenth centuries were all accidental, with no thought that double stars were more than optical coincidences. Halley's observation in 1718 that some

stars were actually in motion probably led to speculations in the middle of the eighteenth century on the existence of systems of stars. In 1767 John Mitchell pointed out that the frequency of occurence of double stars was much too high to be accounted for by the probability of chance. Mitchell's younger contemporary, W. Herschel, remained unconvinced, but finally in 1803 (Herschel 1803) conceded that some double stars were indeed true binaries.

After Herschel, the list of visual double stars continued to grow through observations made by many astronomers, notably F.G.W. Struve in Russia and S.W. Burnham in the United States. These wide pairs of stars (i.e. resolvable through a telescope) for which orbital elements and trigonometric parallaxes are available, are important sources for the determination of stellar masses. These stars do not influence each other except for their mutual gravitational attraction, and thus behave as mass points. Of increasing interest to the modern astronomer are those pairs in which the separation of the components becomes roughly comparable to the stellar size--these are termed 'close' pairs, and cannot be visually resolved. However, other methods of observation have revealed many of these close binaries.

In the latter part of the seventeenth century the star Algol (Al Ghul, as it was named by the people of the ancient Near East) was noted as having variable brightness.

Finally in 1782-3, John Goodricke observed Algol, realized the short periodicity of its brightness, and postulated that this variability was due to "... the interposition of a large body revolving around Algol..." (Goodricke 1783). However, only in 1889 (Vogel 1890) when Algol was recognized as a spectroscopic binary having times of conjunction coincident with times of minimum light, were Algol and similar variable stars recognized as binary systems. β Lyrae was also discovered by Goodricke in 1784 to be a light variable, and was thus the second eclipsing binary to be recognized.

Classification of Binary Stars

There are three classes of binary stars, and a given system may be a member of one, two, or even three of the classes. The first class is composed of systems whose components are far enough apart to be optically resolved, called 'visual' binaries. Direct observations of their apparent positions can be made with a telescope and/or on photographic plates. Other double stars are either too far away from Earth and/or too close to each other to be visually double. The second class can be detected by the wavelength shifts in spectra giving a periodic variation of the radial velocity (or velocities), and are called 'spectroscopic' systems. The third class is identified by photometric observations of periodic variations in the light emitted, and are called

'eclipsing' binaries. These three classifications, however, are not mutually exclusive. For example, a spectroscopic binary which has an appropriate orbital inclination can in principle also be observed as an eclipsing system. The type assigned a binary system in this way is thus dependent on its distance from Earth, and there is much overlap. However, any binary system is completely specified by seven parameters: the mass, radius, and luminosity of each component, and the mean distance between their minimum and maximum separation.

A different method of classification was proposed by Kopal (1955), based on the theoretical upper limit to the size a star can reach in the presence of a companion. This size is usually thought of as the first of the zero-velocity curves of the restricted three-body problem, called the critical surface, and the maximum volumes attainable are the 'Roche lobes'. The relative dimensions are completely specified by the ratio of the two masses, and systems are classified according to whether or not one or both of the components fill their respective Roche lobes. This classification uses information on the masses and radii of the components.

The term 'close binary system' (as opposed to 'wide') usually refers to one in which one component affects the evolution of the other, and thus is closely related to Kopal's classification. In normal stellar

evolution, the radius of the evolving star increases, and thus in a binary system the natural radius may attempt to exceed its Roche lobe, so that the two stars will affect each other's evolution. In this sense close binaries encompass visual, spectroscopic, and eclipsing systems, and are directly involved with the evolutionary history of binaries. The variety of observed binaries is due to the fact that at different stages one of the components (the more massive) fills its Roche lobe.

The recognition of a visual binary depends on the separation of its components and its distance from the Sun. Thus, visual binaries must be relatively near neighbours, within a few hundred parsecs. Spectroscopic binaries can be recognized out to a few thousand parsecs with high dispersion spectrographs. Beyond this limit only eclipsing binaries can be detected (if the eclipses are fairly deep) and thus their recognition in galactic clusters can aid in the determination of the distance to the particular cluster. If the age of the cluster can be found from its colour-magnitude diagram, a check can be made on theories of evolution of close binaries. Spectroscopic binaries which, due to orbital inclination, are also eclipsing have been the main source of information on individual stellar dimensions and masses, leading to the empirical mass-luminosity relationships. If the parallax of a system is also known, the effective temper-

atures of the stars can be determined. Such data provide the basis for studies of stellar structure.

Orbital Elements

The orbit of a binary system is completely defined by seven elements, of which the period is the most important because the generalized form of Kepler's Third Law relates the period P to the semi-major axis a, and to the stellar masses:

$$\frac{a^3}{P^2} \propto (M_1 + M_2) \qquad (1.1)$$

Thus, the following quantities will completely specify the system (Batten 1973):

P : the orbital period, expressed in days for spectroscopic or eclipsing binaries, or in years for visual binaries

i : the inclination of the orbital plane to the tangent plane to the sky

Ω : (applicable only to visual binaries) the position angle, measured from north towards east, of the line of nodes joining the intersection of the orbital and tangent planes, measured in the tangent plane

ω : the longitude of periastron, which is the angle between the directions of the ascending node (where the star crosses the tangent plane moving away from the observer), and of the point of periastron

(the point of closest approach of the two stars). It is measured in the orbital plane in the direction of orbital motion. Visual binaries have ω given for the secondary (fainter) component, but spectroscopic and eclipsing systems specify ω for the orbit of the primary component--the two differ by 180°

a : the semi-major axis of the relative orbit (usually in astronomical units or kilometers)

e : the eccentricity of the orbit, ranging between zero (for a circular orbit) and one (for a straight line)

T : the time of periastron passage, usually expressed as a Julian date

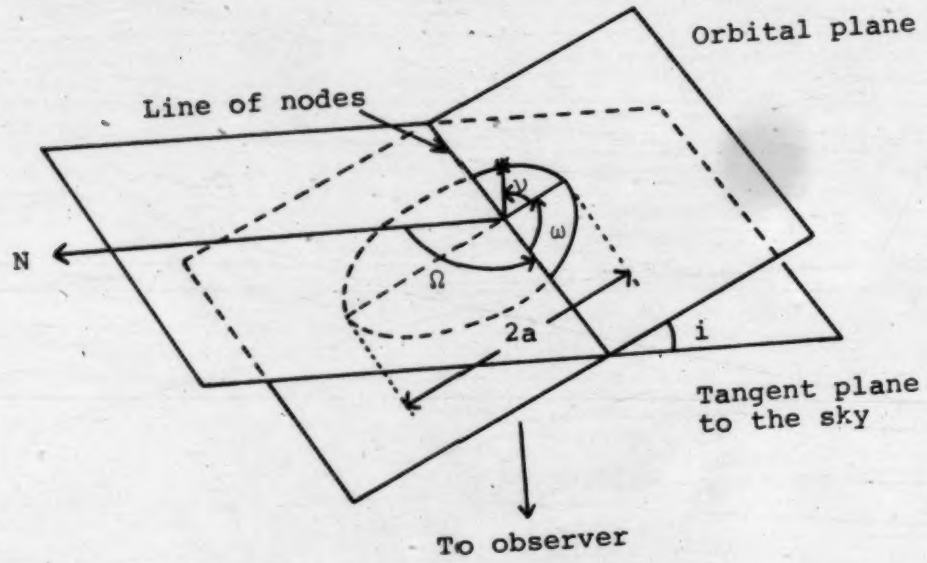

Fig. 1. Orbital elements (from Batten 1973, p. 8)

Determination and Significance of Orbital Elements

For a visual binary the elements P, i, ω, e, and T can be found. The ascending and descending nodes cannot be distinguished unless there are also radial velocity measurements, so there is an uncertainty of 180° in Ω. Usually i is taken to be between 0° and 90° if the apparent motion is direct (i.e. in the direction of increasing position angles); otherwise i lies between 90° and 180°. The ascending node is assumed to be that node for which $\Omega < 180°$. The apparent semi-major axis in seconds of arc can be derived, but an absolute value is not available unless the distance to the system can be independently determined. Radial velocity data can give the scale (relative size) of the orbit, and thus the distance can be determined. Using Kepler's Third Law, assuming normal masses for the spectral type of each component, the major axis (and the distance) can be estimated. This distance estimate expressed as a parallax is called the dynamical parallax. The periods of visual binaries are usually very long (years), and so period determinations are often uncertain, based on only one arc of the curve.

In addition, for a visual binary, the relative brightness of, or the difference in magnitude between, widely separated components can be measured photometrically but, until recently, the systems with orbital periods short enough to allow other element determinations had

such small angular separation that accurate magnitude differences could not be obtained.

Elements determined for spectroscopic binaries are different, and the amount of information depends on whether the spectra of both components are visible (a double-lined spectroscopic binary), or the spectrum of only the brighter component (a single-lined spectroscopic binary) is visible. Usually if the two stars differ by more than about one magnitude, only the spectrum of the brighter star is visible. The period can be determined (see Chapter 3) for either case, and from the shape of the velocity curve the eccentricity, e, and the longitude of periastron, ω, can be found. In addition, γ, the radial velocity of the centre of mass of the system (also known as the systemic velocity), and K_1, half the total range of the radial velocity variation of the brighter companion, are obtained from the velocity curve. The radial velocity reaches its maximum at the ascending node and its minimum at the descending node. The observed velocity contains the velocity of the system as a whole as well as the velocity of the individual components. From the definition of K_1, the quantity $a_1 \sin(i)$ can be calculated, where a_1 is the semi-major axis of the absolute orbit of the brighter star. In addition, if the spectrum is double-lined, K_2 and $a_2 \sin(i)$ for the fainter star can also be found. Using Kepler's Third Law, for a

single spectrum binary, a quantity called the 'mass function', f(M), can be calculated:

$$f(M) = \frac{M_2^3}{(M_1+M_2)^2} \sin^3(i) = 1.035\times10^{-7} K_1^3 P(1-e^2)^{3/2} \; M_\odot \quad (1.2)$$

where P is in days and K is in km/s. Double-lined spectra will give the ratios

$$\frac{a_1}{a_2} = \frac{K_1}{K_2} = \frac{M_2}{M_1} \quad (1.3)$$

and thus the reduced masses

$$M_{1,2}\sin^3(i) = 1.035\times10^{-7} K_{2,1}(K_1+K_2)^2 P(1-e^2)^{3/2} \; M_\odot \quad (1.4)$$

can be determined. Here (K_1+K_2) is proportional to the semi-major axis projected onto a plane containing the line-of-sight, and $(a_1+a_2)=a$. If, as is generally the case, the fainter star is also the less massive, then minimum values of the reduced masses are:

$$M_{1,2}\sin^3(i) = 4f_{1,2}(M) \quad (1.5)$$

For double-lined spectroscopic binaries, the relative intensities of the lines are directly proportional to the stellar luminosities. Petrie (1939; 1950) developed methods of measuring the intensities and thus obtaining the luminosities via the relative depths or equivalent widths of selected spectral lines. However, difficulties may arise if the two stars are of very different spectral types, or if the line profiles in the spectra are of dif-

ferent shapes, or if (as in early-type stars) the lines are very broad and so not properly resolved.

From the light curves, the periods can be found for eclipsing binaries. The minimum distance between the two stars projected onto the plane of the sky is related to the inclination of the orbit, which affects the shape and depth of the light curve. The angle Ω is indeterminate, since the direction of motion of the eclipsing star cannot be found (except through radial velocity measurements). The absolute size of the orbit, a, cannot be found unless spectroscopic data are also available. However, the shape and length of the eclipses depend on the relative radii of the stars in terms of their separation, and these fractional radii can be determined from the light curve. If spectroscopic observations are available, the absolute radii can be calculated. If both eclipses are observable, the displacement between them as a fraction of the period is proportional to $e\cos(\omega)$ to a first approximation when e is small. Short period eclipsing binaries usually have nearly circular orbits. For circular orbits or elliptical orbits with the major axis along the line-of-sight, $e\cos(\omega) = 0$, and the secondary eclipse occurs half-way between two primary eclipses. The difference in the durations of the primary and secondary eclipses, relative to the period, is proportional to $e\sin(\omega)$ when e is small. Thus, e and ω can in principle

be separately determined, but usually the value of $e\sin(\omega)$ has a large uncertainty.

For an eclipsing binary, the combined light of the two stars outside eclipse is taken as the unit of light. If one eclipse is total (a deep, flat-bottomed minimum), the relative luminosities are determined, since the depth of totality gives directly the magnitude difference of the two stars. For partial eclipses (assuming a nearly circular orbit--as is usually the case), the same area of each star is eclipsed and the ratio of the depths of the two eclipses gives the ratio of the surface brightnesses. When the radii are calculated from the shape of the light curve, the ratio of luminosities can then be determined, expressed at one wavelength. If measurements are made at different wavelengths, the results can be used to find the difference in spectral types, thus adding to or confirming the spectroscopic data.

In addition, the limb-darkening of the eclipsed star can be determined by its effect on the shape of the light curve. However, accurate calculations are difficult, since it affects only the small portion of the curve when the limbs of the star are being covered or uncovered. Also, in principle, the distortion of the components in an eclipsing system can be determined, since during times of eclipse the ellipsoidal star shows less surface area than outside eclipse. However, the

observed variations in light between eclipses also involve other complications such as gravity-darkening, tidal distortion, reflection effects, and the presence of circumstellar matter. The point on a distorted star closest to the observer will not be the geometric centre of the apparent disc, so the centre of maximum light is displaced from the star's centre of mass. Thus, the light changes expected within and between minima are very complicated and difficult to interpret.

Selection Effects

For visual binaries, the most important factor affecting their discovery is the distance from the Sun. Thus, the observed frequency of visual binaries appears to be higher among stars of later spectral type, because hot, luminous, early-type stars are scarce in the solar neighbourhood. Another consideration is the magnitude difference between the components: a very luminous star will more likely have a much fainter companion, while a fainter star would have a companion of similar luminosity. Therefore, again, visual binaries are harder to detect among the more luminous stars.

The larger the changes in velocity, the easier it is to detect a spectroscopic binary. Thus, it is easier to detect spectroscopic binaries among more massive systems which have larger velocity variations for a given period and inclination, since orbital velocity is propor-

tional to $(\text{mass})^{1/3}$. The more massive stars are usually the hot luminous ones. Systems of later spectral type stars have generally longer periods, and since velocity variation is inversely proportional to the period, these systems would be more difficult to detect. However, the velocity of early-type stars whose spectra contain few diffuse lines is more uncertain than for later-type stars which exhibit many sharp spectral lines. Thus, more long period systems with low velocity amplitudes will be observed among late spectral type stars. Because double-lined spectra can be observed only in systems where the luminosities of the two components are similar (Δm less than about one magnitude), the masses and absolute dimensions are only available for those systems whose mass ratios are near unity. Some systems have orbital elements (e.g. e, ω, K) which make detection difficult. Therefore, in any group, the number of observed spectroscopic binaries will be underestimated, an effect more important for early-type stars with lower accuracy in their velocity determinations. Double-lined and single-lined binaries have different probabilities of discovery, since double-lined binaries are detected from the spectral line doubling while single-lined systems are detected through velocity changes.

The probability of detecting eclipsing binaries depends on the amount of time the light is less than max-

imum--that is, on the orbital period and duration of eclipse as a fraction of that period--, on the depth of the minima, and on the apparent brightness of the system. The depth and duration of the eclipse are determined in turn by the relative radii and luminosities of the components. A system of two similar stars, which display two equal eclipses, is harder to detect, because the light cannot vary by more than about $0^{m}.75$, and also because the eclipses will more likely be only partial. The geometric probability, i.e. the probability that a system will be inclined so as to show an eclipse, is higher for systems containing a giant or super-giant than those with main-sequence stars. But these eclipsing systems containing widely disparate components are generally the longer period binaries, and it has been shown that long period eclipsing binaries have a low probability of being photometrically detected.

Due to selection effects, double-lined spectroscopic binaries tend to be found among the hotter, more massive stars. Therefore, our knowledge of masses greater than 1 $M_{\odot}$ derives largely from spectroscopic eclipsing systems. Few stars with masses greater than 2 $M_{\odot}$ are found in visual binaries. The determination of masses from eclipsing systems is subject to the uncertainty in sin(i). However i must be fairly large to allow eclipses to occur, and sin(i) is not very sensitive to

the value of i for i close to 90°. Thus, the major uncertainty in masses is due to the uncertainty in K_1 and K_2.

Velocity Curve Distortion: The Rotation Effect

Three types of disturbance in the radial velocity curves of eclipsing spectroscopic binaries have been identified, and they are frequently discovered from the fact that the value of the eccentricity from radial velocity measurements is not the same as that from photometric observations. The three effects are the rotation effect, the presence of gas streams in the system, and the reflection effect. Of these, the rotation effect is of primary interest to this study because of its manifestation in the radial velocity curve of DE Draconis. This effect occurs at the time of eclipse: as one side of the rotating star is eclipsed, effective centres of the spectral lines are shifted according to the direction in which the still exposed limb is rotating. At mid-eclipse, equal areas of both limbs are exposed, so the effect cancels. After mid-eclipse the lines are shifted in the other direction, as more of the one limb is uncovered while the other is eclipsed. As more of the disc of the eclipsed star appears, the effect from each side cancels. The lines become more symmetrical until outside eclipse the lines lie once more at the wavelength corresponding to the line-of-sight velocity of the star. Spectroscopic evidence has

shown that stars in a binary system generally rotate in a direct sense with an angular velocity ω which is equal to the Keplerian orbital angular velocity, or sometimes much larger: in circular orbits, synchronism usually exists between the rates of rotation and revolution, while in eccentric orbits the rotation rate is generally faster than the revolution rate. For a rigid spherical rotator of radius R and equatorial angular velocity ω, a quantity known as the 'rotation factor' ($= \frac{\delta V}{\omega R}$) can be calculated as a function of phase for a given orientation of the axis of rotation to the orbital plane, from elements of the system determined from spectroscopic and photometric data. The quantity δV is the difference at that phase between the observed radial velocity and the calculated, or expected, radial velocity for purely orbital motion. The rotation factor is symmetrical with respect to the moments of conjunction when the eclipse starts and ends, if the rotation axis is perpendicular to the orbital plane. For partial eclipses, it vanishes at mid-minimum, and is equal but of opposite sign before and after. For total eclipses, it becomes $\pm\sin(i)$ at the inner contacts. The symmetry disappears if the axis of rotation in inclined from the perpendicular, and the asymmetry should vanish and reappear periodically in the opposite direction as the axis of rotation precesses under the gravitational influence of the companion.

From the numerical calculations of the rotation factors and the observed δV for each phase, the equatorial velocity ωR for the star can be calculated. If ω is assumed to be the same as for the Keplerian orbital motion (synchronous rotation and revolution), the absolute value of the radius R can be calculated. The axial rotation of a star will cause the spectral line profiles to be broadened by an amount determined by the maximum difference in radial velocity at opposite limbs of the star. If the stars are spherical, the broadening is symmetrical with respect to the centre-of-mass velocity position. However, in a close binary system, the distortion of the stars due to various effects causes the line profiles to broaden and become asymmetric; and if a spherical rotating star undergoes an eclipse, the lines will be asymmetric as well.

Previous Work on the Rotation Effect

The fact that the rotation of an eclipsing binary could produce a measurable effect was recognized by Holt (1893), Schlesinger (1909), and Forbes (1911). Its effect in producing contradictory results from spectroscopically versus photometrically derived orbital elements was shown by Hellerich (1922; 1924). He demonstrated that the discrepancy could often be removed by excluding from the solution spectrograms taken during primary eclipse. The first actual isolation and measurement of the rotation

effect in stellar spectra was done by Rossiter (1924) in β Lyrae, when he recognized it as a way of determining the dimensions of an eclipsing system. A few months later McLaughlin (1924) substantiated the rotation effect in Algol, and subsequently studied it in α Coronae Borealis (McLaughlin 1934a), and in λ Tauri, δ Librae, and RZ Cassiopeiae (McLaughlin 1934b).

Equations for the calculation of the rotation factor for uniformly bright spherical stars were derived by Petrie (1938). Equations which would include limb-darkening were presented by Kopal (1942a; 1942b) who, in the process, introduced and developed a set of functions he called 'associated α-functions', which are generally applicable to an analysis of other effects inherent in observed light curves. Up to this point, no account had been taken of the fact that the axis of rotation could be inclined from the axis of orbital motion, although the above authors were aware that it would have an effect. Then Kopal (1945) made a fuller analysis which took this into account, and subsequent authors (Hosokawa 1953; Kitamura 1953) have extended and refined the calculations.

CHAPTER II

OBSERVATIONAL TECHNIQUES

The spectroscopic eclipsing binary DE Draconis = HD 193964 has been observed at the David Dunlap Observatory (Toronto), and the Dominion Astrophysical Observatory (Victoria), and the spectrograms obtained have yielded the radial velocities used in determining the final orbit. This chapter discusses the methods of observing binary systems, in particular spectroscopic and eclipsing systems. The theory behind using spectrograms to measure radial velocities, the spectral lines that should be seen, the method of reduction, and some sources of error are also discussed.

Some Basic Theory

The basis of radial velocity investigations is the existence of the well-known Doppler-Fizeau principle, which is applied to the component of a star's motion along the line-of-sight, also called its radial velocity. The change in wavelength $\Delta\lambda$ is proportional to the true wavelength λ and the ratio of the relative velocity of the star and the observer, V_r, to the velocity of light, c:

$$V_r = \frac{c\Delta\lambda}{\lambda} \qquad (2.1)$$

The velocity is positive if the star is receding from the

observer (the observed wavelength is longer), and is negative if the star is approaching the observer (shorter wavelength). Reliable values of V_r depend on the accurate determination of the true wavelengths, λ, and the precise measurement of $\Delta\lambda$.

Most stars have absorption line spectra, where the light emitted by the hotter lower photosphere passes through the cooler upper photosphere. The wavelengths of the absorption lines indicate which elements are present in the atmosphere. The lines from the star's spectrum are compared with those of a known source. This is usually an iron arc or an iron-argon hollow cathode tube, whose light passes over the same path in the spectrograph as the light from the star. This comparison spectrum is recorded on each side of the stellar spectrum.

The Spectrograph

Most radial velocity results for early-type stars are based on spectra covering wavelengths from 3800 to 5000 Å. The slit of the spectrograph is illuminated by the image of the star, and it will be most efficient if the slit encompasses the complete image. However, a wide slit reduces the spectral purity, which is measured by the width of the projected image of the slit at the recording device (photographic plate). The resolving power of the spectrograph is usually limited by the slit width and not by the dispersing element.

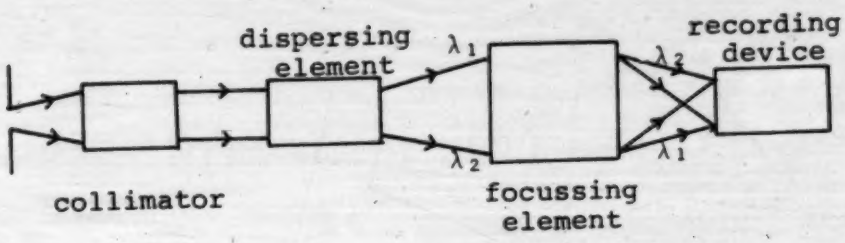

Fig. 2. Schematic diagram of a spectrograph (from Underhill 1966).

The effective speed of a spectrograph is dependent on the ratio of the collimator's diameter to the diameter of the telescope objective, and also on the ratio of the collimator focal length to the camera focal length. The optimum design is to use a large aperture, long focal length collimator and a short focal length camera. For high resolution, high linear dispersion, gratings are used as the dispersing element. The recording device is usually a photographic plate or film, with the requirement that the projected slit width be greater than the size of the photographic grain (emulsion), about five microns. The plates do not have a linear response to various light intensities, so an intensity calibration spectrum is exposed with every spectrogram for light intensity studies. A comparison with the reference spectrum external to the stellar source shows the displacement of the lines on the

stellar spectrum caused by the Earth's motion, the star's motion, and possibly stellar atmospheric motion.

Stellar Spectrograms

Radial Velocity Calculations

Determining the wavelengths from spectrograms involves measuring the position of the stellar lines with respect to the comparison spectrum and interpolating. This procedure involves the following steps. The relation between the wavelength and the positions of lines in the comparison spectrum is called the dispersion curve, and is given by:

$$s-s_o = \frac{\lambda-\lambda_o}{D} \qquad (2.2)$$

where s is the position of the line of wavelength λ, and λ_o, D, and s_o are constants. For grating spectrograms, D is the linear dispersion in angstroms per unit setting. A single set of constants for a given spectrograph can be used over a range of about 200 Å by making use of a correction curve. The settings for three lines of known wavelengths, one at each end and one in the middle of the region, are determined, and the constants λ_o, D, and s_o are calculated. Then the positions of standard wavelengths in the comparison and typical stellar spectra are calculated, with the zero-point of the scale set by making a certain position correspond to a selected wavelength in the comparison spectrum; for this study the zero-point

was the line λ4200 for DAO plates, and λ3927 for DDO plates.

To calculate the radial velocity of the star, the following procedure was used. On each spectrogram, the positions of both the standard wavelengths and the stellar spectral lines are measured after setting the zero-point. At DAO the comparison spectrum was from an iron-argon tube while at DDO an iron arc was used. The measured positions of the comparison lines will not be the same as the calculated ones, so a correction curve for the spectrogram is drawn of the difference Δs versus wavelength. It turns out to be approximately parabolic for grating spectrographs. Then for each stellar line, the correction to the measured setting at that wavelength is read off this curve and applied to the measured position. The difference between the measured positions of the stellar lines and the calculated positions for zero velocity are a measure of the star's motion. These differences are converted to a velocity by the factor DV_s, where D is as in equation 2.2 (i.e. the slope of the dispersion curve at that wavelength), and V_s is the factor $\frac{c}{\lambda}$:

$$V_r = D\Delta s \frac{c}{\lambda} = \Delta\lambda \frac{c}{\lambda} \qquad (2.3)$$

which is the Doppler-Fizeau principle. Then, for each stellar line on the spectrogram, a V_r is obtained. The average of these is taken for one plate, to obtain a

calculated $\overline{V}_r$ for that phase in the star's motion.

However, this calculated velocity is made up of the star's radial velocity with reference to the Sun, plus the component of the Earth's motion in the line-of-sight. The latter involves three components: (1) the Earth's revolution around the Sun; (2) the Earth's daily rotation on its axis; and (3) the motion of the Earth about the centre of mass in the Earth-Moon system. The last of these three components can usually be omitted, being of the order of ±0.014 km/s. The other two can be computed readily (Underhill 1966), with the correction for the Earth's rotational motion varying typically from a few hundredths to a few tenths of a km/s. In addition, if a prism spectrograph is used, a correction for the curvature of the spectral lines must be included and is characteristic of that spectrograph. With most grating spectrographs, no such correction is required, because the images of a long slit are usually straight lines.

In order to monitor the stability of the spectrograph and of his measuring/reduction techniques, and to permit intercomparison with results obtained elsewhere, an observer normally records spectra of one or more 'standard velocity stars' each night.

Standard Wavelengths

It is most important that accurate zero-velocity wavelengths be determined which will be valid for a given

dispersion, applicable over a range of spectral types, and representative of the main part of the stellar atmosphere. Most stellar spectrograms of high dispersion and high resolution show many lines from the atoms and ions in the atmosphere. In early-type spectra, however, there are only a few strong,relatively broad lines; the others are weak and shallow. Some of the strong lines are formed in the surface layers of the atmosphere, and their position in the spectrum may represent the peculiar differential motions of these layers, rather than the motion of the whole star.

Each spectrograph, with its own optical combination and dispersion, will have its own most suitable lines because different dispersions cause different line-blendings. The procedure of calculating appropriate standard B-type stellar wavelengths for each combination of spectrograph-telescope-camera involves a series of steps which work down from well-established wavelengths in solar-type spectra to well-behaved B-type control stars. First, a set of solar wavelengths is determined whose accuracies can be checked by comparing the radial velocities calculated using these values, with the velocities calculated from positional astronomy. The second step is to extend the system to earlier types using control stars of types A and F whose true radial velocities are known. These control stars either belong to clusters whose motions are

known from positional calculations and radial velocities of solar-type stars, or are components of wide binary systems, having a companion of type K5 to F4, and small relative orbital motion. The third step is to extend the set of wavelengths to B-type stars through control stars with radial velocities known by other means. For example, the control stars are members of visual binaries with a companion of type A0 or later, or are members of a cluster with known radial velocity. For the B-type stars, standard laboratory wavelengths are initially used, and the control stars indicate the suitability of each line, its stability and usefulness for main-sequence or supergiant stars. Difficulties arise from the diffuseness of lines in B-type spectra, and from the fact that one-half of the known B-type stars are spectroscopic binaries or have large scale atmospheric motions. Most of the suitable lines are due to HeI and hydrogen, and cover the range of about λ3600 to λ4900.

Interpolation to obtain the corrections to the measured stellar line positions also calls for stable accurate wavelengths in the comparison spectrum. These are called secondary standards, and Class A secondary standards are determined to an accuracy better than 0.0001 Å, and can serve as substitutes for the primary standard which is a line from Kr^{86} with $\lambda 6057.80210_5$ in a vacuum. This defines 1 Å as 10^{-10} meter exactly.

Class B secondary standards are most usually used, and allow the measurement of lines to better than a 0.01 Å accuracy. The wavelengths have an accuracy of at least 0.001 Å. They can be lines of an iron arc in air (which are rather broad) or, more desirably, iron lines emitted in hollow cathode discharges or high-frequency discharges using Ne, Ar, or He as the carrier gas. The standard wavelengths used in reducing the DAO plates, obtained with the spectrograph-telescope combination described in Chapter 3, were calculated as outlined by Batten (1976).

CHAPTER III

THE SPECTROGRAPHIC ORBIT OF DE DRACONIS

This chapter discusses the main features of the spectroscopic eclipsing binary system DE Draconis. The methods used to determine the period and final orbital elements, along with the relevant data, are outlined, and the results are compared with those from the previous research efforts of Hube (1973) and Willmarth (1976). In addition, certain elements are compared with those obtained from photometric observations. The photometric data will be used to calculate such physical parameters for both components as masses, radii, and size of orbit. The graph of the final velocity curve will also show all observational data and the deviations of the observed data during eclipse from the calculated values.

Period Determination

In calculating the elements of a spectroscopic binary, an accurate determination of the period is the first and most crucial requisite. This can be very difficult because an astronomer is restricted by the weather, the location of the telescope, and the allocation of telescope time from obtaining many observations at short, equal intervals. There is no general method for determining the period, and all methods for a preliminary value

are based on trial and error. With computers, the number of trials made is increased and the length of time required to complete the calculations greatly reduced. An unknown number of cycles will occur between different observations at recognizable phases, e.g. maximum or minimum velocities, so that short periods are most difficult to recognize. The basic method is to pick out the maxima and minima from the series of observations at different times. Each corresponding pair of maxima or minima will give a relation:

$$t_2 - t_1 = nP \qquad (3.1)$$

where n is an integer. A number of pairs will give different multiples of the period P, and the smallest common to all is taken as the preliminary value. There will usually be several values, multiples of P, which will satisfy the observations. For each possible value, the phase of each observation is calculated and the observations are plotted to determine of it generates an acceptable curve. In cases where it is difficult to choose, observations must be made on certain critical dates when the alternative periods predict very different velocities. However, even after eliminating all the identifiably unsuitable values, the remaining period may not be the true value. One serious problem is that in the case of spectroscopic binaries, spurious periods may arise from restrictions in the observing program. For example, with

any one telescope and location, observations are often restricted to certain periods of the year. Furthermore, these observations are also restricted to intervals of about one sidereal day (±0.1 day), because measurements are usually taken when the system is near the meridian. Tanner (1948) has proposed a method of detecting spurious periods and this method was used by Hube (1973) in his original determination of the period of DE Draconis.

Determination of Other Orbital Elements

Once the preliminary value of the period has been found, a consideration of the amplitude and shape of the best-fitting curve of velocity versus phase allows the determination of the elements of the true orbit of the star with respect to the centre of gravity of the system: e, ω, T, K, and γ. In addition, the projected semi-major axis asin(i) and the mass function f(M) can be calculated from the orbital elements. The resulting phase-velocity diagram will be sinusoidal unless e is large. The observed,or line-of-sight component of, radial velocity with respect to the Sun consists of the constant velocity of the binary system's centre of mass, γ, plus the variable orbital velocity of the star. Applying the equations of elliptic motion (Underhill 1966; Aitken 1964), the final result is:

$$V_r = \gamma + K[e\cos(\omega) + \cos(\nu+\omega)] \qquad (3.2)$$

where ν, called the 'true anomaly', is the angle from periastron to the star's position in its true orbit at any time t, measured in the direction of motion (see figure 1). Also, the element K can be expressed in terms of P, asin(i), and e.

Preliminary values of K, e, ω, ν (which will give T), and γ can be determined through direct methods (Underhill 1966; Aitken 1964) using the initially determined period P and the observed velocity data. These preliminary elements are then refined by a least-squares solution, which involves the simultaneous adjustment of the five parameters (or six if the period is also varied), since $V_r = f(\gamma, K, e, \omega, T, P)$. For each time of observation the difference in velocity ΔV_r (sometimes denoted by O-C) is the observed velocity minus the calculated velocity for that phase, and this difference is produced by corrections to the elements of $\Delta\gamma$, ΔK, ...

$$\Delta V_r = \frac{\partial f}{\partial \gamma} \Delta\gamma + \frac{\partial f}{\partial K} \Delta K + ... \qquad (3.3)$$

Assuming all the changes, or corrections, are independent and small enough to include only first-order terms, the well-known equation of condition can be applied to each observation (Lehmann-Filhés 1894; Schlesinger 1908). Briefly the steps are the following: (1) the preliminary elements are used to calculate the radial velocity for the phase of each observation; (2) the co-efficients $\frac{\partial f}{\partial \gamma}$,

$\frac{\partial f}{\partial K}$, ... of the differential corrections are computed for each observation, using the residuals O-C from the preliminary values in step (1); (3) normal equations are formed and solved simultaneously to give the differential corrections which are applied to the initial elements. These steps are re-applied any number of times to obtain the required precision. In this study, the values were taken as the final orbital elements after five iterations, and each observation was given equal weight.

Problems arise in the above method when the eccentricity is small. For a circular orbit, $e = 0$, and both T and ω have no significance. When e is small, T and ω are almost indeterminate because the co-efficients of ΔT and $\Delta\omega$ in the Lehmann-Filhés' equations approach one, and a denominator in the solution of the normal equations is almost zero. Fixing T or ω biases the solution and gives unrealistic values of the precision of the elements. Sterne (1941) resolved this difficulty by using the date T_o, the epoch of mean longitude, instead of T. T_o is the date at which the mean longitude $(\omega + M)$ is zero, where M is the mean anomaly, defined by:

$$M = \frac{2\pi}{P} (t - T) \qquad (3.4)$$

and t is the date of observation. The mean longitude at t is then $\frac{2\pi}{P} (t-T_o)$, and T_o remains determinate even for $e = 0$. When e is small but non-zero, a modification of

Schlesinger's least-squares method to correct T_o, instead of T, can be used. But if e is nearly zero the preliminary value is taken to be e = 0, and the simple modification cannot be used. Instead, allowing e to be zero initially, leads to new equations of condition which are solved by least-squares methods. Thus, modifications to e are calculated and then the first procedure can be applied. The second method, that of correcting an initially circular orbit, is particularly applicable to DE Draconis, which has a very small eccentricity.

Previous Orbital Elements of DE Draconis

Although DE Draconis = HD 193964 = HR 7792 [α (1950) = $20^h\ 18^m.8$, δ (1950) = +62°05', m_v = +5.72, B9V] has been known to be a spectroscopic binary system since the early part of this century (Plaskett and Young 1919), the first set of published orbital elements was presented by Hube (1973). Hube determined a preliminary period using 28 spectrograms from the David Dunlap Observatory and four velocities from Victoria and, because the radial velocity curve indicated a low eccentricity, initially determined the best-fitting circular orbit. Employing Sterne's (1941) method, corrections to the circular orbital elements were calculated, and the corrected values were then used as the preliminary quantities in the application of Schlesinger's method (1908). Hube's final elements are given in table 1. Hube used Tanner's method

(1948) to detect any spurious periods but obtained negative results. Willmarth (1976) performed an independent spectroscopic investigation of DE Draconis using eleven velocities from earlier investigations plus fifteen new velocities from the Ritter Observatory. The Willmarth results are also shown in table 1.

Comparison of the two sets of elements shows large differences in the systemic velocity and the semi-amplitude. Hube (1976) obtained another solution using all the published velocities to that date, in which the period was $5^{d}.298095 \pm 0.000025$. Hube pointed out, as he had in his original paper (Hube 1973), the need to clarify the scatter of the observed radial velocities near the time of conjunction, which was larger than would have been expected from internal errors.

Fuertig (1975) found DE Draconis to be an eclipsing binary and, using Hube's (1973) period and working with Mueninger (Fuertig and Mueninger 1976), made further observations of the primary minimum (a transit). The preliminary photometric elements derived by Fuertig and Mueninger are presented in table 2. Fuertig and Mueninger concluded from these elements that the invisible companion is a solar-type star, as expected from Hube's (1973) spectroscopic observations. No secondary minimum was observed.

TABLE 1

THE ORBITAL ELEMENTS

		Hube (1973)		Willmarth (1976)	
Period	P(days)	5.298111	±0.000021	5.29807	±0.00003
Systemic velocity	γ(km/s)	-7.8	±1.3	-1.1	±1.1
Semi-amplitude	K(km/s)	49.7	±2.0	53.8	±2.2
Eccentricity	e	0.037	±0.007	0.0 (assumed)	
Long. of periastron	ω(°)	291.166	±1.973	-	
Periastron passage	T(J.D.)*	1140.485	±0.029	2377.408	
asini	(10^6km)	3.61	±0.13	3.92	±0.16
Mass function	f(M) ⊙	0.067	±0.007	0.085	

*2440000.+

TABLE 2

PHOTOMETRIC ELEMENTS

Co-efficient of limb-darkening of large star	x_g	0.5
Ratio of radii	k	0.35
Radius of large star (a = 1.0)	r_g	0.157
Radius of small star (a = 1.0)	r_s	0.055
Inclination of orbit plane	i (°)	86.85
Eccentricity	e	0
Period	P (days)	5.2984

New Observations

During 1976 and 1977 a total of 87 useful new spectrograms of DE Draconis were obtained: one at the David Dunlap Observatory (DDO) and the remainder at the Dominion Astrophysical Observatory (DAO). These spectrograms were augmented with 18 higher dispersion plates from the DDO that Hube gathered between 1970 and 1972 for his original calculations. The DDO observations were obtained with the grating spectrograph on the 1.88m reflector telescope, giving a dispersion of 12 Å/mm. Typically, on these plates between six and twelve lines could be measured, all plates having similar internal probable errors. The DAO plates were taken with the 21121 spectrograph at the Cassegrain focus of the 1.8m telescope,

giving a dispersion of 15 Å/mm. On these spectrograms usually from six to ten lines could be measured, and all plates had internal errors similar to those from the DDO plates. Thus, all velocities were given equal weight. The DAO plates were measured with the oscilloscope comparator at Victoria and reduced using the standard wavelengths for this system as published by Batten (1976). These observations are documented in Appendix A.

Standard velocity stars were observed on each night as well, and the calculated velocities of these stars indicated that a correction of +1.7 km/s should be added to the velocities obtained from the DAO plates. The observations in Appendix A from the DAO include this correction factor.

New Orbital Elements

In deriving orbital elements, all those velocities obtained during eclipse (phase about $1^d.7$ to $2^d.0$) were omitted, resulting in 52 of the total 105 observations being used. The method of Lehmann-Filhés was applied over five iterations to obtain differential corrections to six elements. The preliminary values used were those of Hube (1973). The resultant period was then fixed, and the remaining five elements were calculated from five iterations of the Lehmann-Filhés equations of condition for five elements. The final values, the mean errors, and Hube's (1973) original solution are listed in table 3.

TABLE 3

FINAL ORBITAL ELEMENTS

		(1978)		Hube (1973)	
Period	P(days)	5.298133	±0.000028	5.298111	±0.000021
Systemic velocity	γ(km/s)	-4.9	±0.4	-7.8	±1.3
Semi-amplitude	K(km/s)	51.2	±0.7	49.7	±2.0
Eccentricity	e	0.025	±0.010	0.037	±0.007
Long. of periastron	ω(°)	323.37	±0.57	291.166	±1.973
Periastron passage	T(J.D.)*	1140.966	±0.008	1140.485	±0.029
asini	(10^6km)	3.73	±0.05	3.61	±0.13
Mass function	f(M) ⊙	0.074	±0.003	0.067	±0.007

*2440000.+

In figures 3 and 4, the observations--the 52 outside eclipse and the 53 during eclipse--have been plotted along with the final velocity curve from the Lehmann-Filhés solution. It shows clearly the rotation effect during the time of eclipse when the smaller (invisible) secondary transits in front of the larger, brighter primary component.

The apparent changes in the orbital elements (see table 3) are probably not real; the earlier velocity measurements were not as carefully controlled with observations of standards as were the later observations. Comparison of the two sets of elements shows that the calculated systemic velocity has apparently decreased, as has the eccentricity. The longitude of periastron has increased but because of the nearly circular orbit, this quantity will be very uncertain. The photometric data of Fuertig and Mueninger (1976) yielded a period of $5^{d}.2984$ and a duration of the eclipse of about 0.06 of a period, or $0^{d}.32$. The times of conjunction should occur $0^{d}.16$ after the start of the eclipse. From the spectroscopic observations in figure 4, the eclipse appears to last from roughly phase $1^{d}.68$ to phase $1^{d}.98$, or about $0^{d}.30$. The time of conjunction, when the curve goes through the systemic velocity line, comes at about phase $1^{d}.83$, or $0^{d}.15$ after the start of the eclipse at phase $1^{d}.68$. Thus, the photometric results and the spectroscopic calculations

Fig. 3. Final velocity curve based on the 52 plates obtained outside eclipse. (See Appendix A for data.) Crosses represent velocities from DDO (Toronto); open circles indicate DAO (Victoria) values.

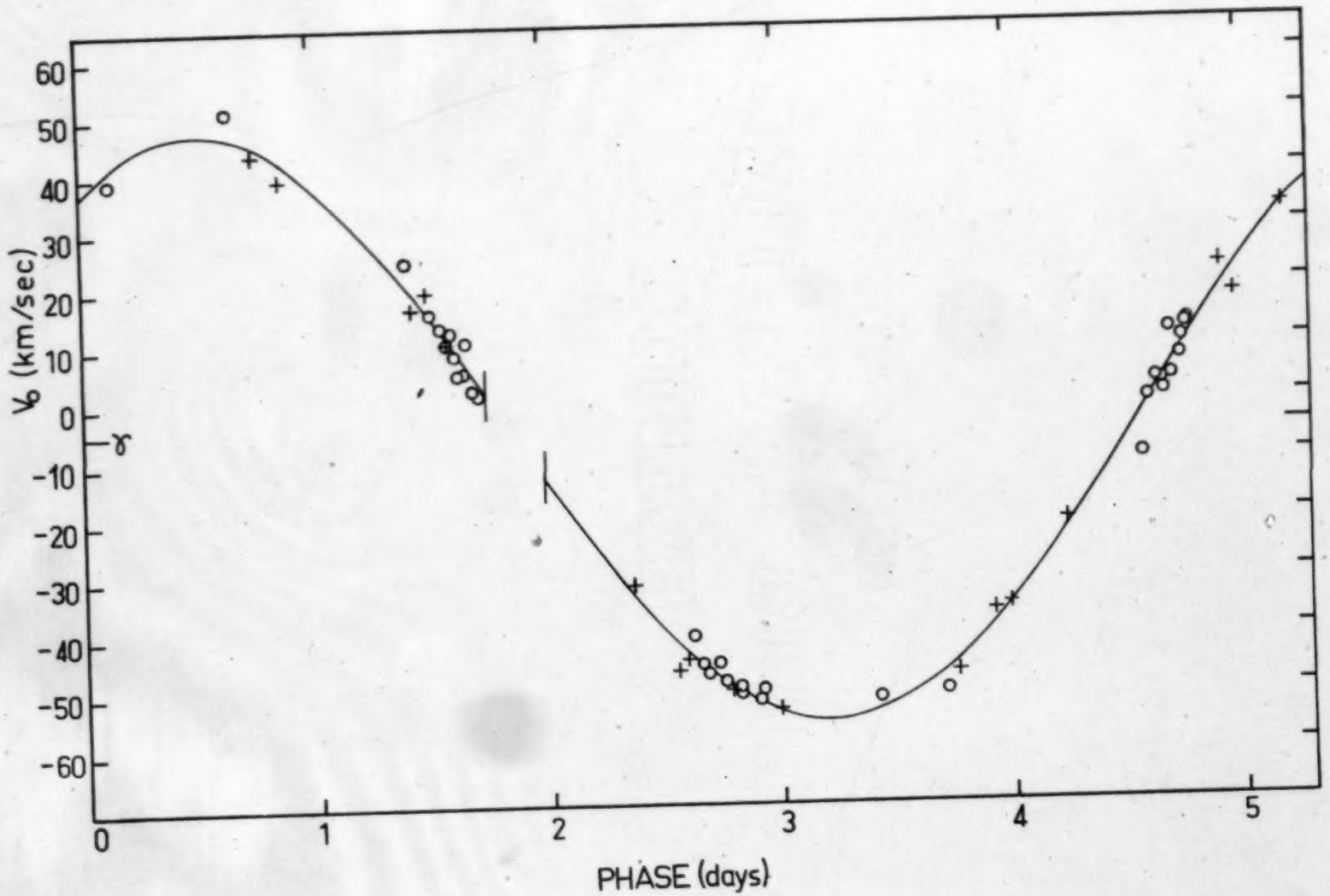
60
50
40
30
20
10
0
-10
-20
-30
-40
-50
-60
V_0 (km/sec)
γ
0
1
2
3
4
5
PHASE (days)

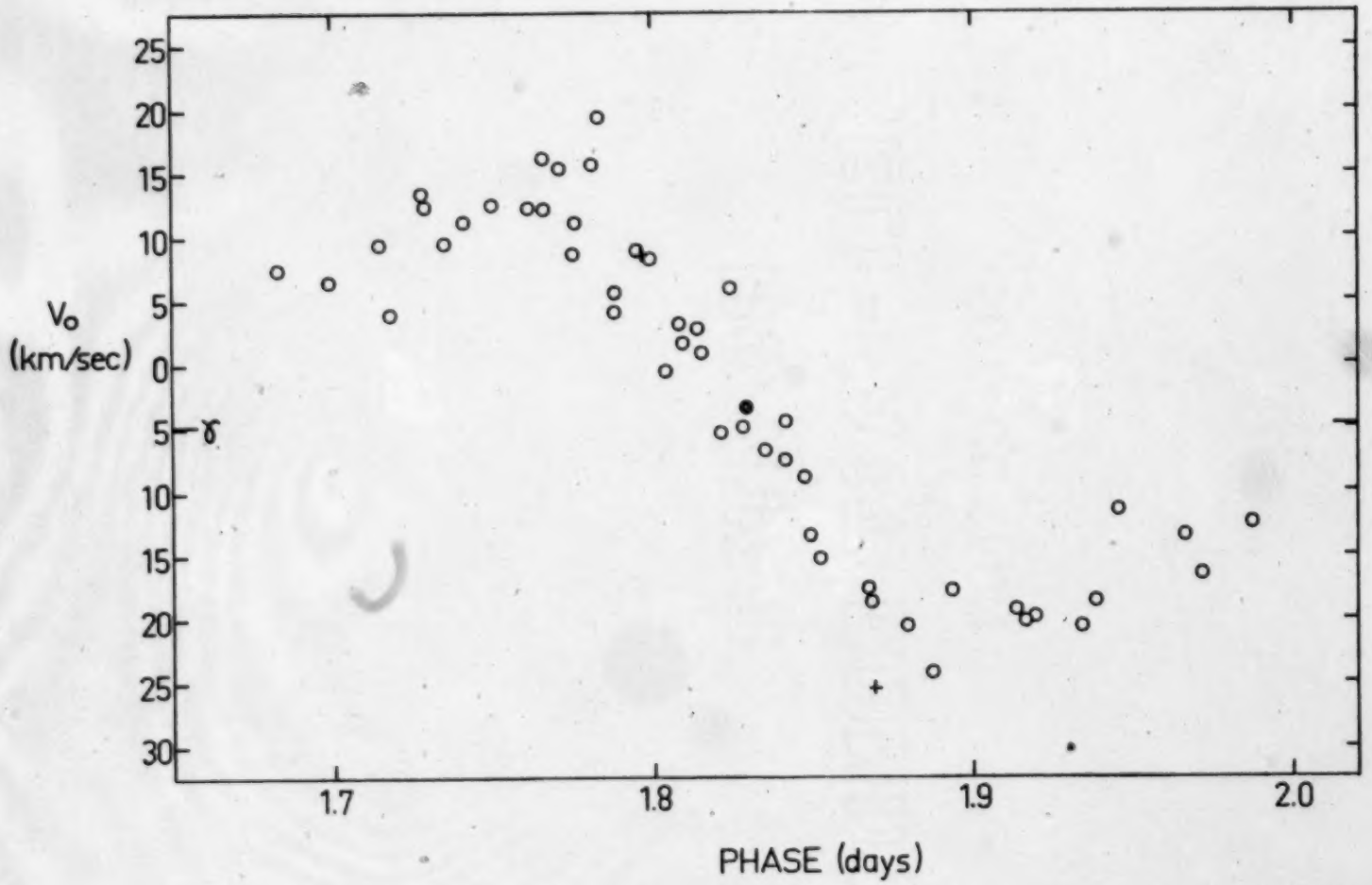

Fig. 4. Observed velocities within eclipse. The 53 points fit in the blank section of fig. 3. Crosses represent DDO velocities; open circles, DAO plates.

show good agreement.

No sure double-lined spectra have thus far been obtained, but there are indications on some plates of line-splitting. Currently, spectrograms of DE Draconis are being obtained during primary eclipse times with a higher dispersion spectrograph on the 48-inch telescope at DAO. Outside of eclipse, the brighter primary overwhelms the secondary, but during the start and end of the eclipse, when part of the primary is blocked off, it is hoped that a higher dispersion will give plates with distinct line structure changes.

Photometric Data and Physical Parameters

Crawford, Barnes, Golson, and Hube (1973) have published results of uvbyβ photometry for DE Draconis and obtained the following parameters: $\beta = 2.824$; $b-y = -0.017$; $m_1 = 0.123$; $c_1 = 0.873$; $V = +5.72$. These colour parameters have been used to calculate some further physical characteristics for DE Draconis. The details may be found in Appendix B, but a brief description of the methods and results is presented here. β is the strength of the Hβ line.

It should be noted that the above data refer to the integrated light from both components. Golay (1972) pointed out that binarity has an effect which is photometrically similar to a small change in spectral type. Theoretically (McNamara 1966; Golay 1974) the effect of adding companions of various masses to primary stars of

different spectral types displaces the colour-luminosity diagram (M_V versus B-V) above and approximately parallel to the main-sequence line appropriate for single stars of the primary spectral types. In a colour-colour diagram (U-B versus B-V), the linear part (primary types B0 to about A5) remains very close to the single star sequence i.e. with the inclusion of a companion, the B-V value remains essentially the same, while the U-B value increases. In the curved part (primary types F0 to G5), the change in the B-V value is more noticeable, while the change in U-B is less so. For DE Draconis, with a primary of type B9V and mass ratio about 3.7 (see Appendix B), the theoretical effect of the secondary on the absolute magnitude and colours assigned to the primary would seem to be unnoticeable, judging from the diagrams and tables given by Golay (1974, pp. 91-93). Also, the following rough calculations will show that in the system the light from the secondary contributes a negligible amount to the total, and therefore the results from the uvbyβ photometry can be assumed to give accurate information on the primary alone.

Assuming the two components of DE Draconis to be B9V and G2V, and using colour and magnitude values appropriate on average for these spectral types, the fraction of light contributed by the secondary at different wavelengths can be calculated from the equation:

$$M_\lambda = -2.5 \log(L_\lambda) \qquad (3.5)$$

and

$$\log \frac{L_{2\lambda}}{L_{1\lambda}} = 0.4(M_{1\lambda} - M_{2\lambda}) \qquad (3.6)$$

where λ is any wavelength, and subscripts 1 and 2 refer to the primary and secondary respectively. The results for UBV wavelengths are shown in table 4.

TABLE 4

FRACTIONAL LIGHT FROM THE SECONDARY
(PRIMARY = 1.0)

	M_V	M_B	M_U	L_{2V}	L_{2B}	L_{2U}
G2V	+4.7	+5.34	+5.50	0.025	0.013	0.009
B9V	+0.7	+0.64	+0.45			

From the above results, it is obvious that the contribution from the secondary at any wavelength in the visible region can be safely ignored, and the uvbyβ data can be assumed to apply to the primary star alone with little or no loss of accuracy.

It is interesting to note here the effect that the axial rotation of the B9V component could have on the colour parameters. Kraft (1970) investigated the influence of rotation on luminosities and temperatures of main-sequence stars. A rotating star which is distorted from a spherical shape has a smaller surface gravity at

the equator than at the poles, so the surface brightness and local effective temperature are lower at the equator than at the poles. Therefore, mean luminosity and temperature are a function of the angle between the line-of-sight and the axis of rotation. Comparing a rotator and a non-rotator of the same mass should in principle show that the rotator has a slightly different luminosity, since the gravitational potential and therefore the central pressure and temperature are changed.

Theoretical results (Kraft 1970; Roxburgh and Strittmatter 1965) indicate that a rotator is cooler than a non-rotator, regardless of aspect, and also that a rotator is brighter (if seen pole-on) or fainter (if seen equator-on) than a non-rotator of the same mass. However, these effects are very small, amounting to at most a few hundred degrees in T_{eff} and a few tenths of a magnitude in M_{bol}. The main sequence for rotating stars is expected to lie to the right of the non-rotator main sequence, with the displacement depending mainly on V^2 (the rotational velocity squared), and not so much on i (the angle between the axis of rotation and the line-of-sight). (See Strittmatter and Sargent 1966; Hardorp and Strittmatter 1968). For early-type stars in the U-B versus B-V diagram, rotation projects stars along the main sequence for non-rotators, rather than at an angle to it. A similar effect occurs in the c_1 versus (b-y) diagram, indi-

cating that rotation does not apparently effect the colour-colour diagrams for early-type stars.

Using a recent calibration of the uvbyβ system (Crawford 1975), the value of c_1 was corrected for reddening to obtain the unreddened parameter c_o for DE Draconis. From Crawford's (1978) calibration of c_o versus β (Zero Age Main Sequence = ZAMS), the value of β for a ZAMS star was determined. Crawford (1978) also calibrated M_V(ZAMS) versus β(ZAMS), and gave a correction term for stars lying above the ZAMS (evolved stars). A value for M_V(ZAMS) was obtained for DE Draconis and corrected for evolutionary effects, since the β(observed) differed from the β(ZAMS). The absolute visual magnitude for DE Draconis was calculated to be $M_V = +0.75$, which compares well with the MK value of +0.6, and also with the value adopted by McNamara (1966) of +0.7.

Crawford's (1975) description of the uvbyβ system also allows the apparent visual magnitude to be corrected for reddening, and from the distance modulus $(m_V - M_V)$, the distance to this system was found to be about 96 parsecs.

Using Crawford's (1978) relation between c_o and $(U-B)_o$, calculations for $\theta_{eff} = \frac{5040}{T_{eff}}$ were made. Several different formulae (Heintze 1973) yielded similar values for T_{eff}, and the finally adopted average value of 11,300°K agrees well with values for spectral type B9V

from other effective temperature versus spectral type scales (e.g. McNamara 1966; Hack and Struve 1969).

From the formula given in Allen (1973), the bolometric correction was calculated, which gave an absolute bolometric magnitude $M_{bol} = +0.19$. The radius was calculated from two different formulae (Allen 1973; Kopal 1959) and the average radius of DE Draconis is 2.2 solar radii. The mass was also calculated using various mass-luminosity relationships (Batten 1968; Allen 1973; Petrie 1950; Harris, Strand, and Worley 1963; Kopal 1959), and the average mass is 2.7 solar masses. These values of mass and radius agree well with those expected for a typical B9V star (see Underhill 1966).

Further results can be found for the secondary component using the mass function, projected semi-major axis, and the photometric elements of Fuertig and Mueninger (1976). From the inclination $i = 86°.85$, the calculated mass of the primary, and the mass function, the secondary is found to be about one solar mass. This is consistent with the expectations from the photometric data of Fuertig and Mueninger (1976) for a solar-type secondary, since no secondary minimum had been observed. It is also in agreement with the spectroscopic observations, where no lines of the secondary were visible. The radius of the relative orbit, $a = a_1 + a_2$, was also calculated, and from the photometrically determined frac-

tional radii, the absolute radii were found to be 3.1 and 1.1 solar radii for the primary and secondary, respectively.

The values of the radii above differ from those obtained using the calculated bolometric absolute magnitude, but still conform within the limits expected for these spectral types. Also, the calculation of M_{bol} is liable to be very approximate because there appear to be many differences of opinion regarding the correct effective temperature calculation, and mass-luminosity relationship. The parameters derived above and some comparison data are summarised in table 5. The values of $R_{1,2}$ shown in brackets were computed using the calculated M_{bol}. The adopted values of 3.1 and 1.1 solar radii were determined using photometric data, and the values for $a_{1,2}$ were calculated using these adopted radii.

TABLE 5

PHYSICAL PARAMETERS OF DE DRACONIS

		Primary (subscript 1)	Secondary (subscript 2)	Typical Values For B9V	Source
Distance	d	96 parsecs	96 parsecs		
Apparent visual magnitude	V	5.72			
Absolute visual magnitude	M_V	+0.75		+0.7	McNamara 1966
Unreddened colour index	$(U-B)_o$	-0.19		-0.19	McNamara 1966
Average effective temp.	T_{eff}	11.3×10^3 °K		11.5×10^3 °K	McNamara 1966
Bolometric correction	B.C.	-0.56		-0.66	Harris 1963
Absolute bolometric magnitude	M_{bol}	0.19			
Average mass	$M_{1,2}$	$2.7M_\odot$	$1.0M_\odot$	$2.63M_\odot$	McNamara 1966
Average radius	$R_{1,2}$	$3.1R_\odot$ $(2.2)_\odot$	$1.1R_\odot$ $(0.8)_\odot$		
Radius of orbit	$a_{1,2}$	3.74×10^6 km	9.99×10^6 km		

CHAPTER IV

THE ROTATION EFFECT

In this chapter we will discuss the distortion of a radial velocity curve of a binary system due to the eclipse of an axially rotating star. Some straightforward effects which can be expected and the general theory required to calculate these effects under certain assumptions will be presented. The results of calculations done for DE Dra, and the implications for certain physical dimensions of this system will be presented.

General Information

Probably all stars rotate, although to varying degrees. For the more rapidly rotating stars the effect shows up in the spectral lines, and the rotational velocity $V_e \sin\alpha$ can be calculated if $V_e \sin\alpha$ is greater than about 25 km/s. (Here α is the angle between the axis of rotation and the line-of-sight). The total light received from a star is made up of contributions from the visible part of the hemisphere. For a single rotating star one limb is approaching the observer, and the other limb is receding. The light from the approaching limb thus shows absorption lines displaced toward the violet, while for the other limb they are dis-

placed toward the red. The overall effect is a set of broadened absorption lines, the widths depending on the star's rate of rotation and orientation. For a rapid rotator the lines are also shallower (less intense) than for a slower rotator because the absorption is spread over a greater region of the spectrum. The centres of the lines are not displaced by the rotation when the whole stellar disc is observed. If the rotating star happens to be a component of an eclipsing binary system, its spectral lines are asymmetrically broadened during the eclipse. The observed velocity is not only the orbital velocity but also includes a contribution from the rotation. If (as is almost always the case) the directions of axial rotation and orbital revolution are the same, then at the start of eclipse the other component will obscure that limb of the rotating star which is approaching the observer. The receding limb (shift to the red) contributes and the apparent velocity is more positive than the calculated orbital velocity. At the end of eclipse only the approaching limb is visible (shift to the violet) and observed velocities are more negative. If the eclipse is total, then the star is not visible for the duration of totality, but just prior to and after totality a thin crescent of the rotating star is seen. In this case even a modest rotational velocity can produce large departures from the expected values. For an annular eclipse (as in DE Dra) a ring of the eclipsed rotating star is always visible and light from one side is at least partly balanced by light from the other.

The effect is thus reduced, however a high rotational velocity will produce a small effect. At the middle of an annular eclipse the opposite sides of the ring exactly balance and the net rotational effect is zero. The central portion of the star, which has no Doppler effect due to rotation but produces a deeper centre of the absorption line, is eclipsed. At this point the absorption lines are shallow, and some may have a central peak as if they were doubled lines. Figure 5 illustrates the eclipse configurations for a transit and the effect on the radial velocity curve. This situation is typified by DE Dra.

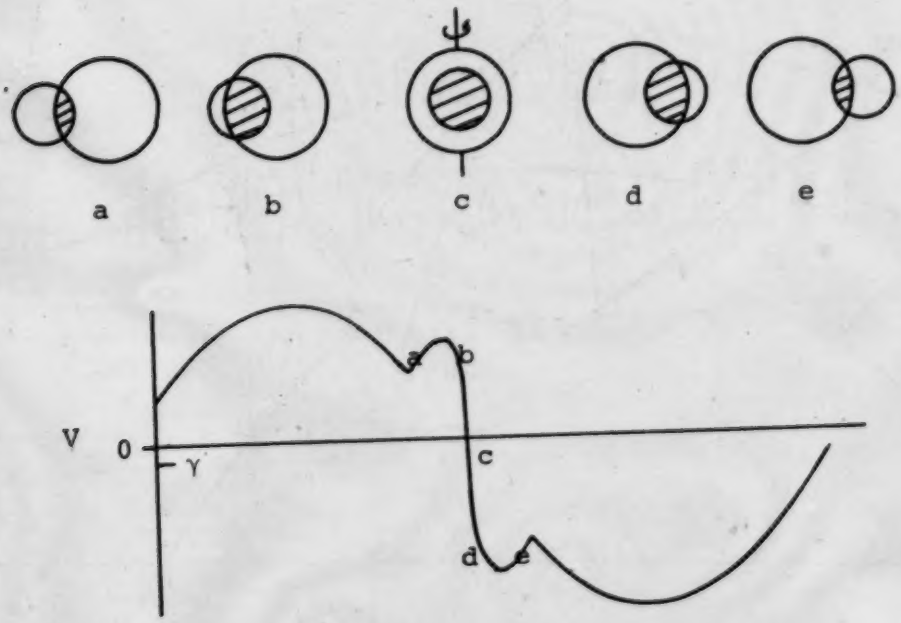

Fig. 5. The configuration for a transit

The observed rotational velocities are the projections on the line-of-sight of the true equatorial velocities: $V_{obs} = V_e \sin\alpha$. If the assumption is made that the axes of rotation are randomly oriented in space then: $\overline{V}_e = \frac{4}{\pi}\overline{V_e \sin\alpha}$. This assumption is justified by agreement of the calculated distribution of $V_e \sin\alpha$ assuming random orientation with the observed distribution of Chandrasekhar and Münch (1950).

Calculations of the rotational velocities from the spectral line shapes have been made for stars belonging to all spectral types and luminosities. The results show that the rotational velocities depend on the spectral type and luminosity. Hack and Struve (1969) present the results of many investigations. In particular it is found that the early-type stars have the largest observed rotational velocities. For main-sequence stars, the values are greatest between types O5 and B5: $\overline{V}_e \approx 160$ km/s (Hack and Struve 1969, fig. 4b). For B9V stars $\overline{V}_e \approx 130$ km/s. However there are stars, notably Be stars and shell stars, with $\overline{V}_e \approx 340$ km/s and 520 km/s, respectively. Slettebak (1966) calculated the break-up velocities--when the centrifugal acceleration becomes equal to the gravitational acceleration--based on certain main-sequence rotating star models. He found that these break-up velocities are higher than the greatest observed rotational velocities: for a B9V star, an estimate from his curve shows V_e(break-up) $\approx 450 \pm 25$ km/s while V_e(max. obs.) $\approx 350 \pm 25$ km/s. The difference between the two curves is a minimum for the earliest B stars and increases with advancing

spectral type.

The rotation of stars which are members of binary systems has also been investigated. Plavec (1970) points out that Plaut (1959) concluded that for systems with orbital periods less than 10 days, the periods of rotation and revolution are usually the same, while for longer periods there is no synchronism and the stars rotate like single objects. Plavec (1970) observed a definite tendency for components of binary systems to rotate more slowly than the average for single stars of the same type. For example, an estimate from his plot yields V_e(single) ≈ 190 km/s but V_e(binary) ≈ 80 km/s. He also plotted actual rotational velocities versus calculated synchronous velocities for close binary systems, $V_{syn} = \frac{2\pi(\text{radius})}{\text{period}}$, and found that synchronism applies at least approximately in most cases. There were no cases where the component rotated much more slowly than was required for synchronism, but a few stars rotated much more rapidly. Plavec also noted that in spectroscopic binaries of short or moderate period, the secondaries, if less than $1M_\odot$, can always be expected to rotate in synchronism with the orbital motion.

The observation that close binaries generally rotate more slowly than single stars is supported by Jaschek (1970). He found for B stars that for members of spectroscopic binaries the largest percentage has $V_e \sin\alpha$ in the range 0 to 100 km/s, while for normal single stars the range with the highest percentage is from 100 to 200 km/s.

As will be seen later, the rotational velocity calculated for DE Dra lies at the upper end of the range expected for single stars, and is also much greater than the synchronous velocity. This contradicts the above general observations. However Nariai (1971) investigated various published rotational velocities for double-lined spectroscopic and eclipsing binaries and found that for normal main-sequence stars as components of double- and single-line binaries the deviation from synchronism is large.

Preliminary Theory

The displacement of a spectral line from its zero velocity position involves contributions to the line-of-sight component from the visible area of the star. The line-of-sight components of velocity of points on a spherical star rotating as a rigid body are the same for all points on a line on the apparent (projected) disc parallel to the projected axis of rotation. Assuming the axis of rotation is perpendicular to the orbital plane ($\alpha = i$), the following definition of the 'rotation factor' is found:

Let dA = area of a strip of the disc parallel to the projected axis of rotation

a = distance of the strip from the axis

i = inclination of the orbital plane to the plane of the sky

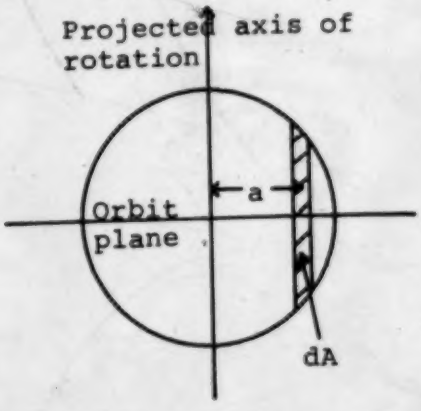

Fig. 6. Projected disc

V_e = rotational velocity of a point on the equator

V_r = line-of-sight component of the velocity of strip dA

Then
$$V_r = V_e \sin i \tag{4.1}$$

and the deviation of the radial velocity from purely elliptic motion of the visible area of the star is:

$$V_{obs} = V_e \sin i \, \frac{\int a\,dA}{\int dA} \tag{4.2}$$

where the integration is over the visible portion only, so that the 'rotation factor' F is:

$$F \equiv \frac{\int a\,dA}{\int dA} \tag{4.3}$$

Thus F is the mean value of the rotational component in the line-of-sight averaged over the visible portion of the star.

Petrie's Analysis

Petrie (1938) performed the above integration for an eclipse of a spherical, uniformly bright, rigidly rotating star in a circular orbit. The origin of the co-ordinate system is the centre of the brighter star and the X-axis is along the line joining the centres of the projected discs. Petrie's basic equation is:

$$F = \frac{\iint \frac{s}{k} dx\,dy}{\iint dx\,dy} \tag{4.4}$$

where s = distance of a point, on the projected disc, from the projected axis of rotation

and k = radius of the small star.

Petrie evaluated the equation for three cases: (1) a small bright star eclipsed by a larger fainter star; (2) a large bright star eclipsed by its smaller fainter companion; and

(3) eclipses of ellipsoidal stars. DE Dra is an example of case (2).

If the radius of the larger brighter star (whose centre is the origin) is unity, the projected distance between the centres is given by:

$$\delta = \frac{1}{r_\ell}\sqrt{\cos^2 i + \sin^2 i \sin^2\theta} \qquad (4.5)$$

where r_ℓ = radius of the large star with respect to the radius of the relative orbit

θ = longitude from mid-eclipse

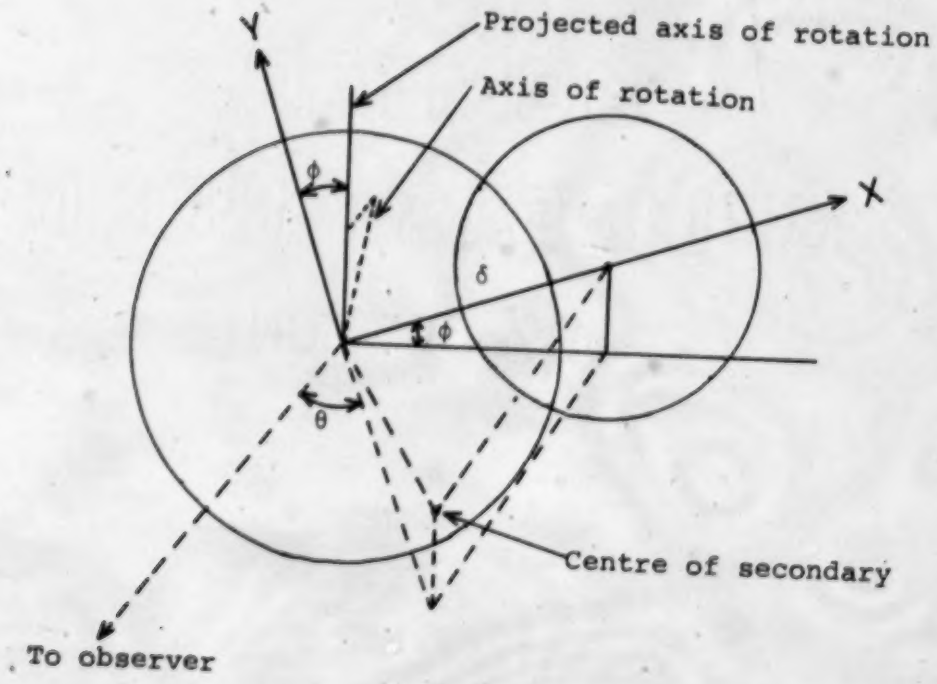

Fig. 7. Projected configuration of eclipse (from Petrie 1938)

The distance s of a point on the primary from the projected axis is then:

$$s = x\cos\phi - y\sin\phi \tag{4.6}$$

where

$$\cos\phi = \frac{\sin\theta}{\delta r_\ell} \quad \text{and} \quad \sin\phi = \frac{\cos i\cos\theta}{\delta r_\ell} \tag{4.7}$$

The boundaries of the projected discs are circles defined by:

$$x^2 + y^2 = 1 \qquad \text{larger brighter star} \tag{4.8}$$

$$(x-\delta)^2 + y^2 = k^2 \qquad \text{smaller fainter star} \tag{4.9}$$

The points of intersection of the two circles have co-ordinates:

$$x_1 = \frac{1 + \delta^2 - k^2}{2\delta} \tag{4.10}$$

$$y_1 = \pm\sqrt{\frac{4\delta^2 - (1 + \delta^2 - k^2)^2}{4\delta^2}} \tag{4.11}$$

The equation for F becomes:

$$F = \frac{\frac{1}{k}\iint(x\cos\phi - y\sin\phi)\,dxdy}{\iint dxdy} \tag{4.12}$$

where in the numerator the x-integration for the visible portion is done first from the limb of the brighter to the eclipsing limb of the fainter. The y-integration then sums these strips from one intersection point to the other. The parts of the disc above and below this cancel each other, and thus appear only in the denominator which must sum over the whole visible part of the star. Therefore three cases arise from this method of performing the integration as illustrated in the following Figures 8a, 8b, and 8c.

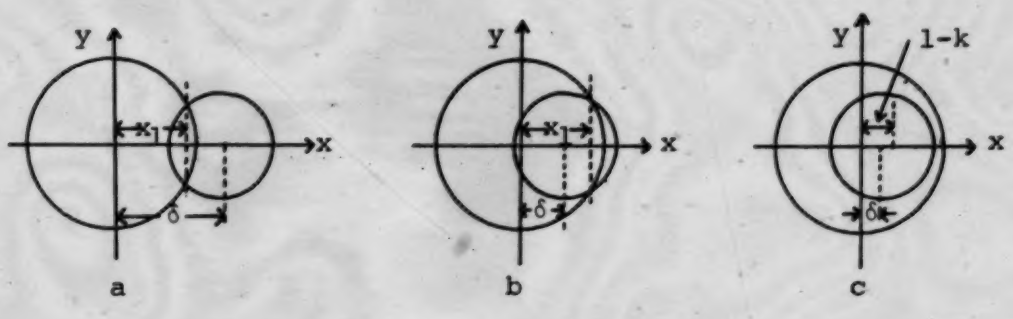

Fig. 8. Configurations for Petrie's three cases

The corresponding formulae are:

Case 1 (Fig. 8a): $x_1 \leq \delta$

$$F = \frac{-\delta\cos\phi \left\{\left(\frac{1-\delta^2-k^2}{\delta}\right)y_1 + y_1\sqrt{k^2-y_1^2} + k^2\sin^{-1}\left(\frac{y_1}{k}\right)\right\}}{\pi + 2y_1\delta - y_1\sqrt{1-y_1^2} - y_1\sqrt{k^2-y_1^2} - \sin^{-1}y_1 - k^2\sin^{-1}\left(\frac{y_1}{k}\right)} \qquad (4.13)$$

Case 2 (Fig. 8b): $1 > x_1 > \delta$

$$F = \frac{-\delta\cos\phi \left\{\left(\frac{1-\delta^2-k^2}{\delta}\right)y_1 + \pi k^2 - y_1\sqrt{k^2-y_1^2} - k^2\sin^{-1}\left(\frac{y_1}{k}\right)\right\}}{\pi(1-k^2)+2y_1\delta-y_1\sqrt{1-y_1^2}+y_1\sqrt{k^2-y_1^2} - \sin^{-1}y_1 + k^2\sin^{-1}\left(\frac{y_1}{k}\right)} \qquad (4.14)$$

Case 3 (Fig. 8c): $\delta \leq 1-k$

$$F = \frac{-k^2\delta\cos\phi}{1-k^2} \qquad (4.15)$$

The results of applying Petrie's analysis to the observational points from eclipse data of DE Dra for several different values of the rotational velocity are shown in Table 6 and Figure 9. There is a large amount of scatter

TABLE 6

ROTATIONAL VELOCITY DATA: PETRIE

PHASE	ROT VEL = 160.0		ROT VEL = 180.0		ROT VEL = 200.0	
	ROT FACTOR	O-C	ROT FACTOR	O-C	ROT FACTOR	O-C
1.796	0.032682	5.22	0.032682	5.87	0.032682	6.53
1.869	-0.044271	-7.07	-0.044271	-7.96	-0.044271	-8.84
1.804	0.024250	3.87	0.024250	4.36	0.024250	4.84
1.841	-0.014762	-2.36	-0.014762	-2.65	-0.014762	-2.95
1.879	-0.054799	-8.75	-0.054799	-9.85	-0.054799	-10.94
1.913	-0.079037	-12.63	-0.079037	-14.21	-0.079037	-15.78
1.987	-0.008783	-1.40	-0.008783	-1.58	-0.008783	-1.75
1.718	0.063938	10.21	0.063938	11.49	0.063938	12.77
1.741	0.079038	12.63	0.079038	14.21	0.079038	15.78
1.773	0.056904	9.09	0.056904	10.23	0.056904	11.36
1.788	0.041110	6.57	0.041110	7.39	0.041110	8.21
1.809	0.018979	3.03	0.018979	3.41	0.018979	3.79
1.828	-0.001055	-0.17	-0.001055	-0.19	-0.001055	-0.21
1.849	-0.023197	-3.71	-0.023197	-4.17	-0.023197	-4.63
1.761	0.069526	11.11	0.069526	12.50	0.069526	13.88
1.766	0.064268	10.27	0.064268	11.55	0.064268	12.83
1.771	0.059008	9.43	0.059008	10.61	0.059008	11.78
1.776	0.053746	8.59	0.053746	9.66	0.053746	10.73
1.781	0.048482	7.75	0.048482	8.71	0.048482	9.68
1.788	0.041110	6.57	0.041110	7.39	0.041110	8.21
1.808	0.020034	3.20	0.020034	3.60	0.020034	4.00
1.815	0.012654	2.02	0.012654	2.27	0.012654	2.53
1.821	0.006326	1.01	0.006326	1.14	0.006326	1.26
1.829	-0.002110	-0.34	-0.002110	-0.38	-0.002110	-0.42

TABLE 6--Continued

PHASE	ROT VEL = 160.0		ROT VEL = 180.0		ROT VEL = 200.0	
	ROT FACTOR	O-C	ROT FACTOR	O-C	ROT FACTOR	O-C
1.835	-0.008436	-1.35	-0.008436	-1.52	-0.008436	-1.68
1.841	-0.014762	-2.36	-0.014762	-2.65	-0.014762	-2.95
1.847	-0.021088	-3.37	-0.021088	-3.79	-0.021088	-4.21
1.852	-0.026359	-4.21	-0.026359	-4.74	-0.026359	-5.26
1.868	-0.043218	-6.90	-0.043218	-7.77	-0.043218	-8.63
1.887	-0.063217	-10.10	-0.063217	-11.36	-0.063217	-12.62
1.893	-0.069526	-11.11	-0.069526	-12.50	-0.069526	-13.88
1.916	-0.078078	-12.47	-0.078078	-14.03	-0.078078	-15.59
1.919	-0.076743	-12.26	-0.076743	-13.79	-0.076743	-15.33
1.934	-0.065800	-10.51	-0.065800	-11.83	-0.065800	-13.14
1.938	-0.062003	-9.91	-0.062003	-11.14	-0.062003	-12.38
1.945	-0.054772	-8.75	-0.054772	-9.84	-0.054772	-10.94
1.966	-0.030905	-4.94	-0.030905	-5.55	-0.030905	-6.17
1.971	-0.025224	-4.03	-0.025224	-4.53	-0.025224	-5.04
1.728	0.072402	11.57	0.072402	13.01	0.072402	14.46
1.795	0.033735	5.39	0.033735	6.06	0.033735	6.74
1.824	0.003163	0.51	0.003163	0.57	0.003163	0.63
1.749	0.079268	12.66	0.079268	14.25	0.079268	15.83
1.766	0.064268	10.27	0.064268	11.55	0.064268	12.83
1.829	-0.002110	-0.34	-0.002110	-0.38	-0.002110	-0.42
1.750	0.078995	12.62	0.078995	14.20	0.078995	15.78
1.783	0.046376	7.41	0.046376	8.34	0.046376	9.26
1.735	0.076743	12.26	0.076743	13.79	0.076743	15.33
1.867	-0.042164	-6.74	-0.042164	-7.58	-0.042164	-8.42

TABLE 6--Continued

PHASE	ROT VEL = 160.0		ROT VEL = 180.0		ROT VEL = 200.0	
	ROT FACTOR	O-C	ROT FACTOR	O-C	ROT FACTOR	O-C
1.814	0.013707	2.19	0.013707	2.46	0.013707	2.74
1.799	0.029520	4.72	0.029520	5.31	0.029520	5.90
1.699	0.043601	6.97	0.043601	7.84	0.043601	8.71
1.715	0.061012	9.75	0.061012	10.97	0.061012	12.18
1.683	0.025224	4.03	0.025224	4.53	0.025224	5.04

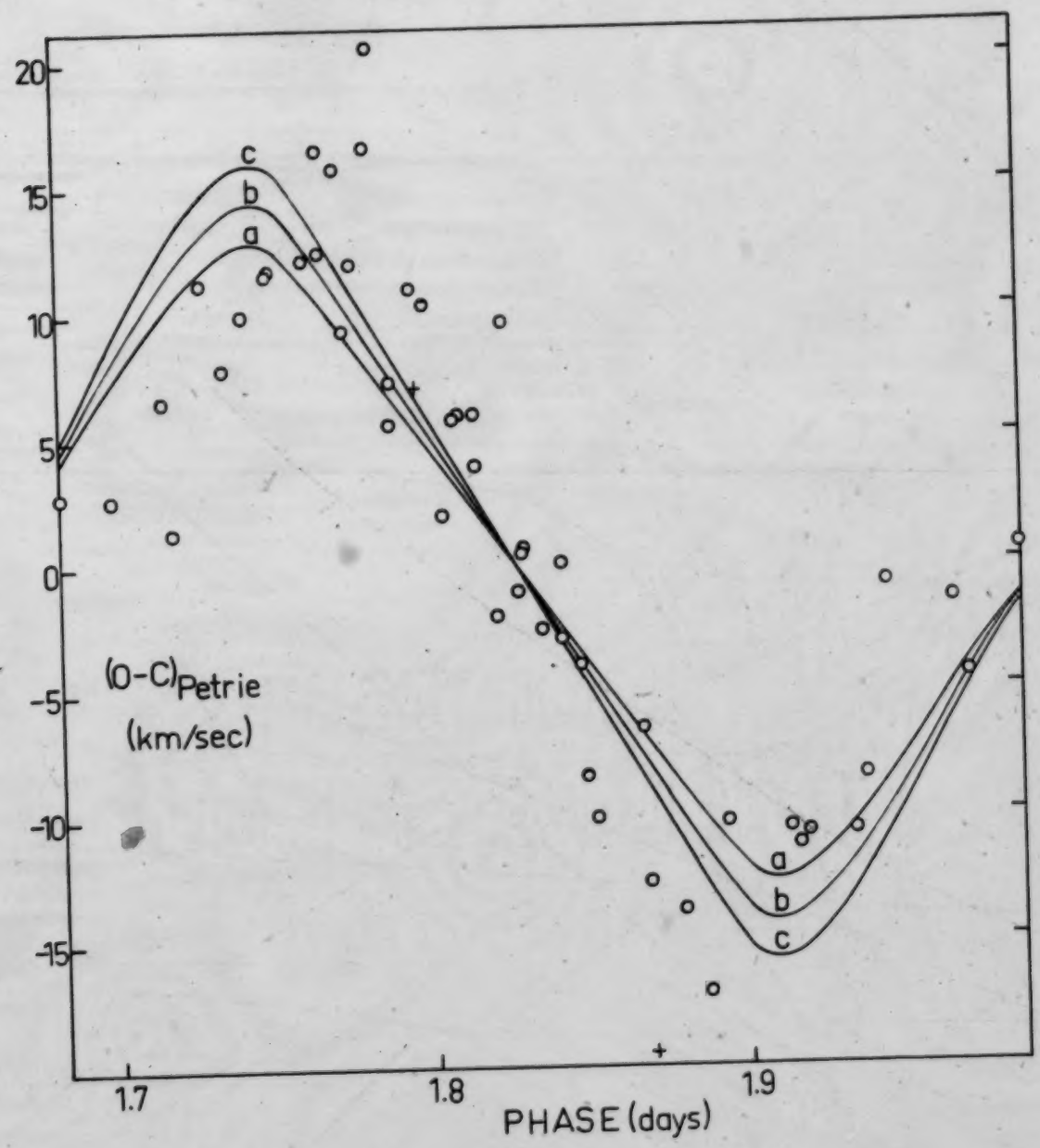

Fig. 9. Calculated rotation curves: Petrie. The results are listed in table 6. The value t(mid-eclipse) = 1.827 days was used to calculate θ, the longitude from mid-eclipse. The curves are based on different values of V_e: (a) V_e = 160 km/s; (b) V_e = 180 km/s; (c) V_e = 200 km/s. Open circles represent observations from the DAO; crosses indicate a DDO plate.

in the data, and the effect seems to be slightly asymmetric. Petrie's analysis does not include the effects of limb-darkening, and assumes that the axis of rotation is perpendicular to the orbit plane. The value of V_e is about 180 km/s judging solely from the maximum and minimum calculated O-C values. Possibly due to other previously mentioned effects, the calculated and observed curves are offset from one another.

Hosokawa-Kopal Analysis

General Theory

Kopal (1942; 1945) rederived formulae for the rotational effect using a more general analysis, and extended it to arbitrarily limb-darkened spherical stars. His solutions were based on the assumption that the star rotates as a rigid body about an axis coincident with the pole of the orbit. However Kopal notes that the two axes need not necessarily be coincident, and Hosokawa (1953) used Kopal's newly developed associated α-functions to obtain formulae for binary systems of spherical stars whose axes of rotation are inclined from the perpendicular to the orbital plane.

For spherical stars rotating as rigid bodies about a fixed axis, the observed radial velocity of a star has two parts: V, due to space and orbital motion; and δV due to the star's axial rotation. The amount δV is found by multiplying the line-of-sight radial rotational velocity V(x,y,z) at any point on the stellar surface by the corresponding element of light dℓ, integrating over the visible portion of the eclipsed

disc, and dividing by the total light from the star. The origin of the rectangular co-ordinate system is the centre of mass of the primary star, i.e. the eclipsed star. The X-axis is constantly in the direction of the centre of the secondary star projected onto the xy-plane (perpendicular to the line-of-sight), and the Z-axis is along the line-of-sight. Then

$$\delta V = \frac{\int\int v d\ell}{\int\int d\ell} \qquad (4.16)$$

For a rigid rotator with constant angular velocity ω, the radial rotational velocity V at any point is proportional to the distance of the point from the axis of rotation projected onto the celestial sphere (xy-plane). Figure 9 shows the configuration and defines the various parameters. Then

$$V = \omega \sin a \{x\cos(\eta+\beta) + y\sin(\eta+\beta)\} \qquad (4.17)$$

For most stars, a linear law of limb-darkening has been found to approximate conditions with a high degree of accuracy; so the distribution of surface brightness is:

$$J = J_o(1 - u + u\cos\gamma) \qquad (4.18)$$

where u is the co-efficient of limb-darkening of the eclipsed star; γ is the angle of foreshortening, i.e. the angle between a surface normal and the line-of-sight or Z-axis; and J_o is the brightness at the centre or the intensity of radiation emerging normal to the surface.

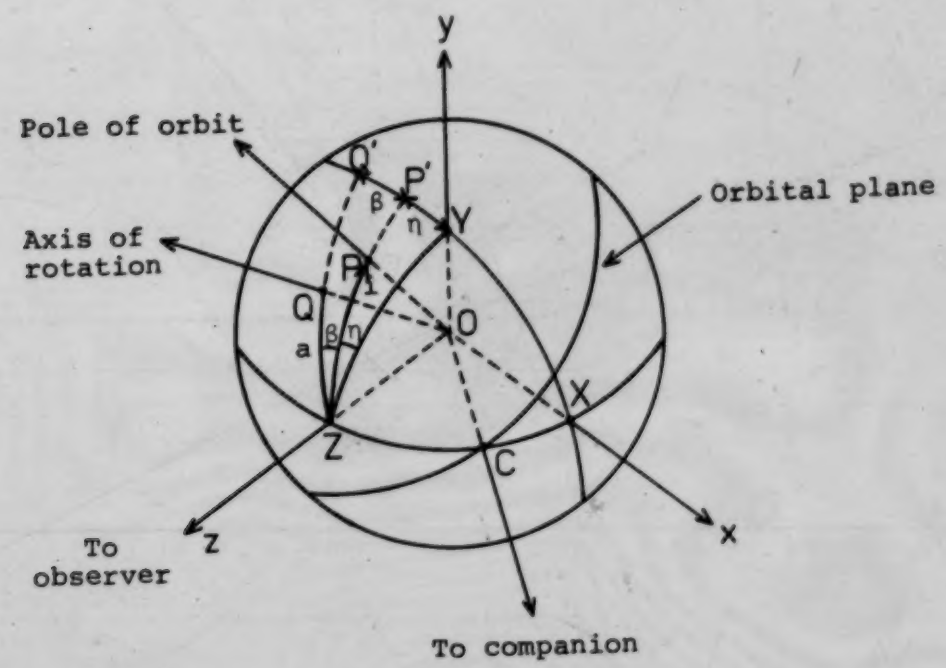

Fig. 10. Configuration and notations for Hosokawa's analysis (from Hosokawa 1953, fig. 1) with the following explanation: (diagram shows the situation just after mid-eclipse)

(x,y): rectangular co-ordinates in plane perpendicular to the line-of-sight, origin at the centre of the eclipsed disc, x-axis in the direction of the projected centre of the companion

i: the inclination of the orbital plane to the celestial sphere

a: the inclination of the axis of rotation to the line-of-sight

η: the angle between the y-axis and the pole of the orbit, projected to the celestial sphere

β: the angle between the projected axis of rotation and the projected pole of the orbit

θ: the phase angle of the companion in the relative orbit (angle ZOC)

δ: the projected separation of the centres of the stars

Directions of rotation and revolution are the same

The limits of the integration are briefly determined as follows. The primary's projected disc is given by:

$$x^2 + y^2 = R_1^2 \tag{4.19}$$

while that of the secondary is:

$$(\delta - x)^2 + y^2 = R_2^2 \quad \text{or} \quad y^2 = R_2^2 - (\delta - x)^2 \tag{4.20}$$

where R_1 = the absolute radius of the primary

R_2 = the absolute radius of the secondary

δ = the projected distance between the centres of the two stars.

During partial eclipse, the two discs overlap and the x-co-ordinate of the common chord joining the two points of intersection is given by:

$$s = \frac{R_1^2 - R_2^2 + \delta^2}{2\delta} \tag{4.21}$$

The double integral is split up into two parts, each bounded by this common chord and the appropriate star's arc: $QR_1Q'S$ and $QR_2Q'S$.

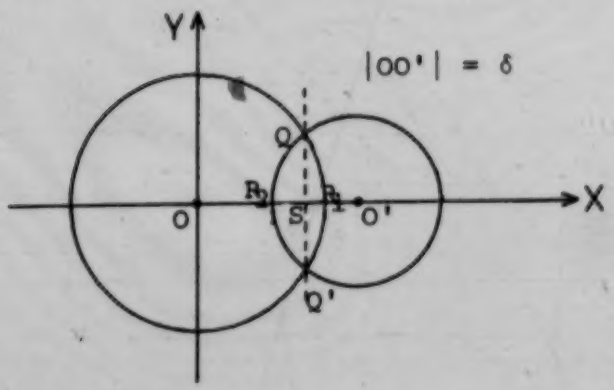

Fig. 11. Limits for eclipse integrals

Letting R_1 denote the absolute radius of the eclipsed star, we see that:

$$R_1^2 = x^2 + y^2 + z^2 \tag{4.22}$$

or $$z = \sqrt{R_1^2 - x^2 - y^2}$$

and $$\cos\gamma = \frac{z}{R_1} \tag{4.23}$$

Then the element of light is given by:

$$d\ell = \frac{J}{R_1}\{R_1(1-u) + uz\}dxdy \tag{4.24}$$

Combining the formulae for V and $d\ell$, and using the fact that $\int ydxdy$ vanishes when integrated over any area symmetrical with respect to the Y-axis, we obtain:

$$\delta V = \omega \sin a \cos(\eta+\beta)\frac{R_1(1-u)\iint xdxdy + u\iint xzdxdy}{R_1(1-u)\iint dxdy + u\iint zdxdy} \tag{4.25}$$

As previously stated, the integrations extend only over the visible portion of the star. It is most convenient to integrate over the whole disc, and subtract the integral over the eclipsed portion. The numerator vanishes when integrated over the whole disc, and the denominator reduces to πR_1^2 and $^2/_3\pi R_1^2$. The remaining integrals then extend over the eclipsed area, and are of the form which Kopal termed his 'associated α-functions':

$$\pi R_1^{m+n+2}\ \alpha_n^m \equiv \iint x^m z^n dxdy \tag{4.26}$$

Then for a partial eclipse the integral becomes:

$$\pi R_1^{m+n+2}\ \alpha_n^m \equiv \left\{ \int_s^{R_1} \int_{-\sqrt{R_1^2-x^2}}^{+\sqrt{R_1^2-x^2}} + \int_{\delta-R_2}^{s} \int_{-\sqrt{R_2^2-(\delta-x)^2}}^{+\sqrt{R_2^2-(\delta-x)^2}} \right\} x^m z^n dxdy \tag{4.27}$$

If the eclipse is total ($R_1 < R_2$) the area $QR_1Q'S$ becomes equal to the whole area of the primary (eclipsed) star, while if the eclipse is annular as for DE Dra ($R_1 > R_2$) the sector $QR_1Q'S$ vanishes and the integral becomes:

$$\pi R_1^{m+n+2}\ \alpha_n^m \equiv \int_{(\delta-R_2)}^{(\delta+R_2)} \int_{-\sqrt{R_2^2-(\delta-x)^2}}^{+\sqrt{R_2^2-(\delta-x)^2}} x^m z^n dxdy \tag{4.28}$$

The associated α-functions of order m and index n all turn out to be functions of two independent variables which are usually taken to be k, the ratio of radii of the two components, and p, the geometrical depth of the eclipse:

$$k = \frac{r_{small}}{r_{large}} \quad \text{and} \quad p = \frac{\delta - r_{large}}{r_{small}} \tag{4.29}$$

where $r_{small,large}$ refer to the fractional radii. By definition k lies between zero and one, while p is normalized to vary from +1 at first contact to -1 at internal tangency (totality or annular phase). All α- functions vanish when $p = 1$; at totality where $R_1 < R_2$ odd orders vanish, while zero

or even orders reduce to constants. However as in DE Dra where $R_1 > R_2$, all α-functions remain finite at the moment of internal tangency.

In terms of the associated α-functions, the formula for the rotation effect becomes (see equation 4.25):

$$\delta V = -R\omega \sin i \cos(\eta+\beta) \frac{(1-u)\alpha_0^1 + u\alpha_1^1}{(1-u)(1-\alpha_0^0) + u(^2/_3 - \alpha_1^0)} \qquad (4.30)$$

Tables of values which enable the calculation of the two lowest functions of zero order, α_0^0 and α_1^0, have been tabulated by Zessewitch (1939; 1940): α_0^0 represents the fractional loss of light during the eclipse of a uniformly bright (u = 0) circular disc (equal to the fractional area eclipsed); $^3/_2\ \alpha_1^0$ represents the fractional loss of light of a circular disc completely darkened at the limb (u = 1). The formulae for the loss of light during any type of eclipse can be set up and evaluated in a closed form. However the explicit forms are so complicated that they are of practical use only when their values are presented in tabular form. For practical reasons the loss of light is normalized to vary between 0 and 1 by dividing by the loss of light at the moment of internal tangency. In Zessewitch's tables the normalized values for arbitrary limb-darkening are denoted as $\alpha^x(k,p)$. In practice all α^x's can be obtained from the appropriate combination of the $\alpha(k,p)$ for a uniform (x = 0) disc and the $\alpha^D(k,p)$ for a completely darkened disc. For the theory and formulae pertaining to eclipsing binary systems see Kopal

(1946). Due to the normalization the tabulated values also depend on whether the eclipse is an occultation or a transit. For a uniform disc the two are related by k^2, but for the darkened case the relationship is more complicated, and separate tables of $\alpha^D(k,p)$ must be used depending on whether an occultation (function α') or a transit (function α'') is observed.

The associated α-functions are a prerequisite for interpreting the rotational effect in close binary systems, for predicting non-radial light or velocity changes, and for interpreting line profiles of distorted stars during and out of eclipse, as well as many other phenomena observed in close binary systems. Kopal investigated these functions in several papers (see e.g. Kopal 1942b; 1945) and in 1947 published a detailed study of the theory and tabulated values of this family of functions. He found that the α-functions of order $m = 0,1,2,3$ could be expressed as simple combinations of certain 'I-integrals' factored by powers of r_2/r_1 and δ/r_2 or s/r_2. The I-integrals involve only one independent variable $\mu \equiv \frac{(\delta-s)}{r_2}$, and so are much easier to tabulate. For each set of indices $I^m_{\beta,\gamma}$, values are calculated for the range of μ, once for partial phases and once for annular phases. From the tabulated values of $I^0_{i,0}$ the values of α^1_0 at each phase are found, while values of $I^0_{i,1}$ yield the appropriate values of α^1_1.

Calculations of α-Functions for DE Draconis

Because of the large number of eclipse data points and the obvious groupings at various phases, it was decided to reduce the 53 observations to a more easily managed set of 15 normal points (simple averages) as shown in figs. 12,13.

The calculations of the required α_0^0, α_1^0, α_0^1, α_1^1 were performed for each normal phase point, in the following steps, with values of k, r_{large}, r_{small}, and u being taken from the photometric results of Fuertig and Mueninger (1976).

1. For each point, the primary's phase in days was converted to true anomaly in the relative orbit, ν, using the spectroscopic value of eccentricity and standard formulae (see e.g. Aitken 1964; Schlesinger 1908)

2. From this calculated value of ν, the true anomaly of the secondary in the relative orbit reckoned from mid-primary minimum, θ, was determined from the relation (recall that ω is the longitude of periastron):

$$\cos\theta = \sin(\nu+\omega) \tag{4.31}$$

3. The value of δ, the projected separation of the centres of the two stars, is given by:

$$\delta^2 = \sin^2\theta\sin^2 i + \cos^2 i \tag{4.32}$$

where i is the inclination of the pole of the orbit from the line-of-sight.

4. The value of the parameter p [$= \frac{(\delta - r_\ell)}{r_s}$] was calculated, and Zessewitch's tables (no. 50, 1940) yielded the value $\alpha(k,p)$ for a uniformly bright disc from which was found

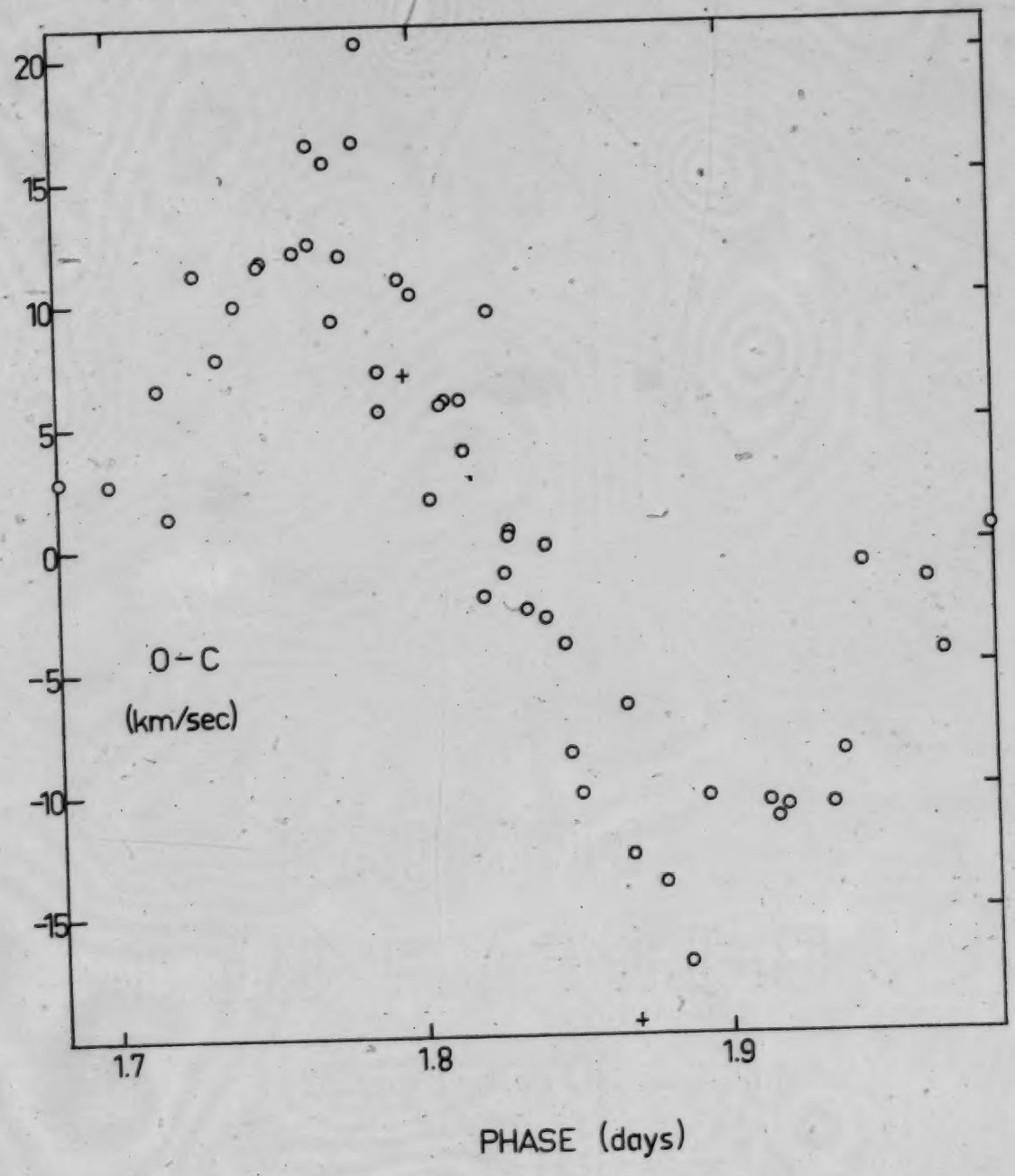

Fig. 12. Eclipse data points. Crosses represent DDO plates; open circles, DAO observations.

Fig. 13. Normal (averaged) points from eclipse points of fig. 12.

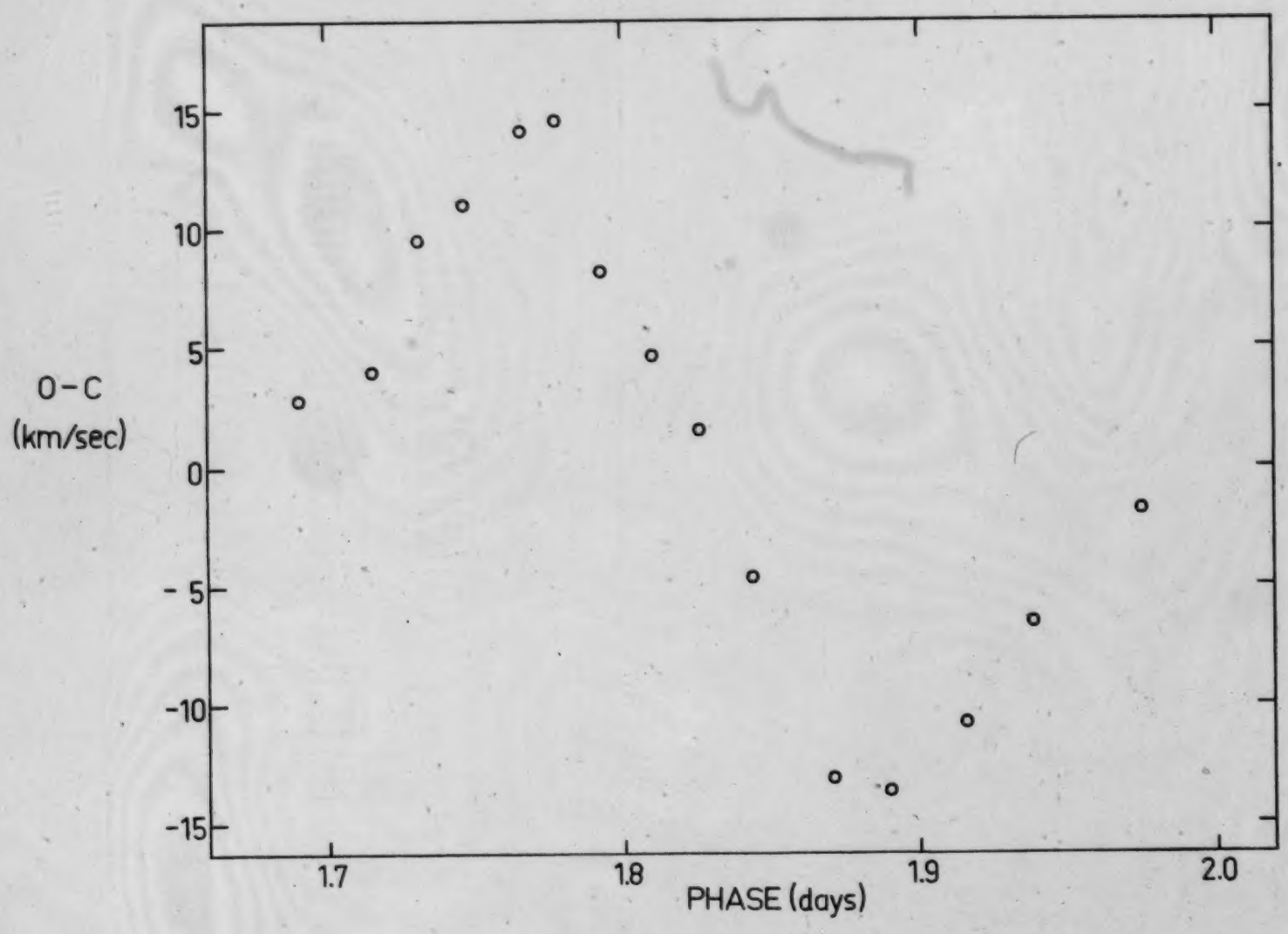
15
10
5
0
- 5
-10
-15
O-C
(km/sec)
1.7
1.8
1.9
2.0
PHASE (days)

$\alpha_o^o = k^2\alpha(k,p)$

5. For partial phases i.e. if $-1 < p < +1$, Zessewitch's tables (no. 45, 1939) for a completely darkened disc gave a value of $\alpha''(k,p)$ and thus $\alpha_1^o = k^2\Phi(k)\alpha''(k,p)$. For annular phases i.e. $p < -1$, the parameter $q = \frac{k(1+p)}{k-1}$ is used for convenience, and since $\alpha(k,p) = 1$ when $p < -1$, $\alpha_o^o = k^2$ for points during annular phase. For a completely darkened disc $\alpha''(k,p) = 1 + A(k)X(k,q)$ during annular phase so that $\alpha_1^o = k^2\Phi(k)[1 + A(k)X(k,q)]$. The functions $\Phi(k)$, $A(k)$, and $X(k,q)$ were tabulated by Zessewitch as well (1940)

6. The evaluation of the higher order functions, α_o^1 and α_1^1, involve the use of Kopal's tabulated I-integrals (1947). This requires the calculation of μ and $D = \frac{\delta}{r_2}$. For convenience Kopal introduces a new variable, a, which is an independent angular variable and a single-valued function of μ. For partial eclipses ($r_1+r_2 > \delta > r_1-r_2$), $a = \cos^{-1}\mu$. For annular phases ($\delta < |r_1-r_2|$), $a = 2\sin^{-1}\frac{2}{1-\mu}$. Then the functions are given by:

$$\alpha_o^1 = 2k^3 D I_{1,o}^o(a) \quad \text{and} \quad \alpha_1^1 = 2k^4 D^{3/2} I_{1,1}^o(a) \qquad (4.33)$$

The values of the I's are given at intervals of 5° in a, so to aid in more precise interpolation than simple linear, the modified second tabular difference M" is given as well. The first four terms of the Everett formula were then used to find the I-values for intermediate angles:

$$I_n = (1-n)I_o + nI_1 + M''_o E''_o + M''_1 E''_1 \quad (0 \leq n \leq 1)$$

The values of the co-efficients E''_o and E''_1 were taken from Thompson (1921).

The Final Formula

From the photometry of Fuertig and Mueninger, the limb-darkening co-efficient u is taken to be 0.5. On substituting this into the rotation effect equation 4.30, it becomes:

$$\delta V = -R\omega \sin i \cos(\eta+\beta) \frac{\alpha^1_o + \alpha^1_1}{\frac{5}{3} - \alpha^o_o - \alpha^o_1} \qquad (4.34)$$

Also from the spherical triangle relations:

$$\cos\eta = \frac{\sin\theta}{\delta} \quad \text{and} \quad \sin\eta = \frac{\cos i \cos\theta}{\delta} \qquad (4.35)$$

Then setting the linear equatorial velocity $V_e = \omega R$ the above expression 4.34 becomes:

$$\delta V = AF\cos\theta - BF\sin\theta \qquad (4.36)$$

where $A = V_e \sin a \sin\beta \cos i$ and $B = V_e \sin a \cos\beta$ are both independent of phase, while

$$F = \frac{1}{\delta} \frac{\alpha^1_o + \alpha^1_1}{\frac{5}{3} - \alpha^o_o - \alpha^o_1} \qquad (4.37)$$

is dependent on phase. The values of the factors involved in F, and the results for each phase angle are presented in Table 7.

In order to fit the observed velocities with some

TABLE 7

ROTATION EFFECT: HOSOKAWA

Phase (days)	δ ($\times 10^{-1}$)	α_o^o ($\times 10^{-1}$)	α_i^o ($\times 10^{-1}$)	α_o^1 ($\times 10^{-1}$)	α_i^1 ($\times 10^{-1}$)	F ($\times 10^{-1}$)	δV_{obs} (km/s)	δV_{calc}			
								$\beta=-10°$	$\beta=0°$	$\beta=+5°$	$\beta=+10°$
1.691	1.675	0.423	0.182	0.368	0.154	1.943	2.75	5.36	5.80	5.94	6.05
1.716	1.403	0.803	0.436	0.634	0.327	4.443	3.95	9.84	10.80	11.15	11.42
1.732	1.246	1.015	0.608	0.751	0.422	6.261	9.50	11.87	13.18	13.69	14.10
1.747	1.089	1.186	0.782	0.810	0.496	8.157	11.07	12.77	14.44	15.12	15.68
1.766	0.907	1.225	0.936	0.707	0.511	9.256	14.15	10.74	12.58	13.37	14.05
1.778	0.802	1.225	0.998	0.625	0.485	9.588	14.60	8.36	10.18	10.97	11.68
1.793	0.686	1.225	1.052	0.535	0.440	9.872	8.22	5.76	7.65	8.51	9.30
1.810	0.590	1.225	1.089	0.460	0.393	10.068	4.68	2.22	4.09	4.98	5.83
1.826	0.550	1.225	1.103	0.429	0.371	10.138	1.48	-1.22	0.61	1.52	2.41
1.844	0.577	1.225	1.094	0.450	0.386	10.092	-4.65	-5.09	-3.33	-2.41	-1.55
1.871	0.733	1.225	1.032	0.571	0.460	9.764	-13.08	-10.53	-8.91	-8.00	-7.03
1.890	0.892	1.225	0.946	0.695	0.508	9.308	-13.65	-13.79	-12.31	-11.43	-10.46
1.916	1.140	1.138	0.727	0.800	0.476	7.560	-10.80	-15.36	-14.22	-13.49	-12.66
1.939	1.375	0.842	0.465	0.658	0.344	4.744	-6.63	-11.93	-11.26	-10.79	-10.25
1.975	1.756	0.319	0.125	0.285	0.109	1.385	-1.80	-4.53	-4.35	-4.21	-4.04

calculated points, various values of β were substituted and an average value of $V_e \sin a$ was found using the observed δV_{obs}. Because the O-C curve is only slightly skew, and the velocity curve itself is quite symmetric, the axis of rotation cannot be radically inclined from the pole of the orbit. Thus we are restricted to small values of β, and values of a close to i [≃ 87°]. The average value $V_e \sin a$ = 188 km/s was used to calculate the expected δV_{calc} for each normal phase point for β = 0°, +5°, ±10°. From the calculated curves in Figure 14 compared with the observed points the best-fit value of β to the maximum and minimum O-C is a small positive quantity of about +5°. As with Petrie's analysis, the calculated curves are off-set from the observed normal points, partly due to some other effects not included in this analysis, e.g. gravity-darkening.

The value of a should not reasonably be less than about 70°, so from $V_e \sin a$ = 188 km/s, the value of V_e could be between about 177 and 188 km/s. By Petrie's previous method, his value of about 180 km/s falls right in the middle of the range expected from Hosokawa's analysis. If a is taken to be the inclination of the orbit, ≃ 87°, then V_e = 188 km/s which is slightly higher than Petrie's value.

Comments

The values from both analyses above fall within the range expected for a single B9V star. However if synchronism is assumed, then the V_e should only be about 30 km/s assuming the radius to be 3.1 solar radii. Obviously the

Fig. 14. Calculated rotation curves: Hosokawa. The data are listed in table 7. The four curves are based on the same value of $V_e \sin a$ = 188 km/s, but different values of β: (a) β = -10°; (b) β = 0°; (c) β = +5°; (d) β = +10°. Open circles represent the normal (averaged) points from the observational data.

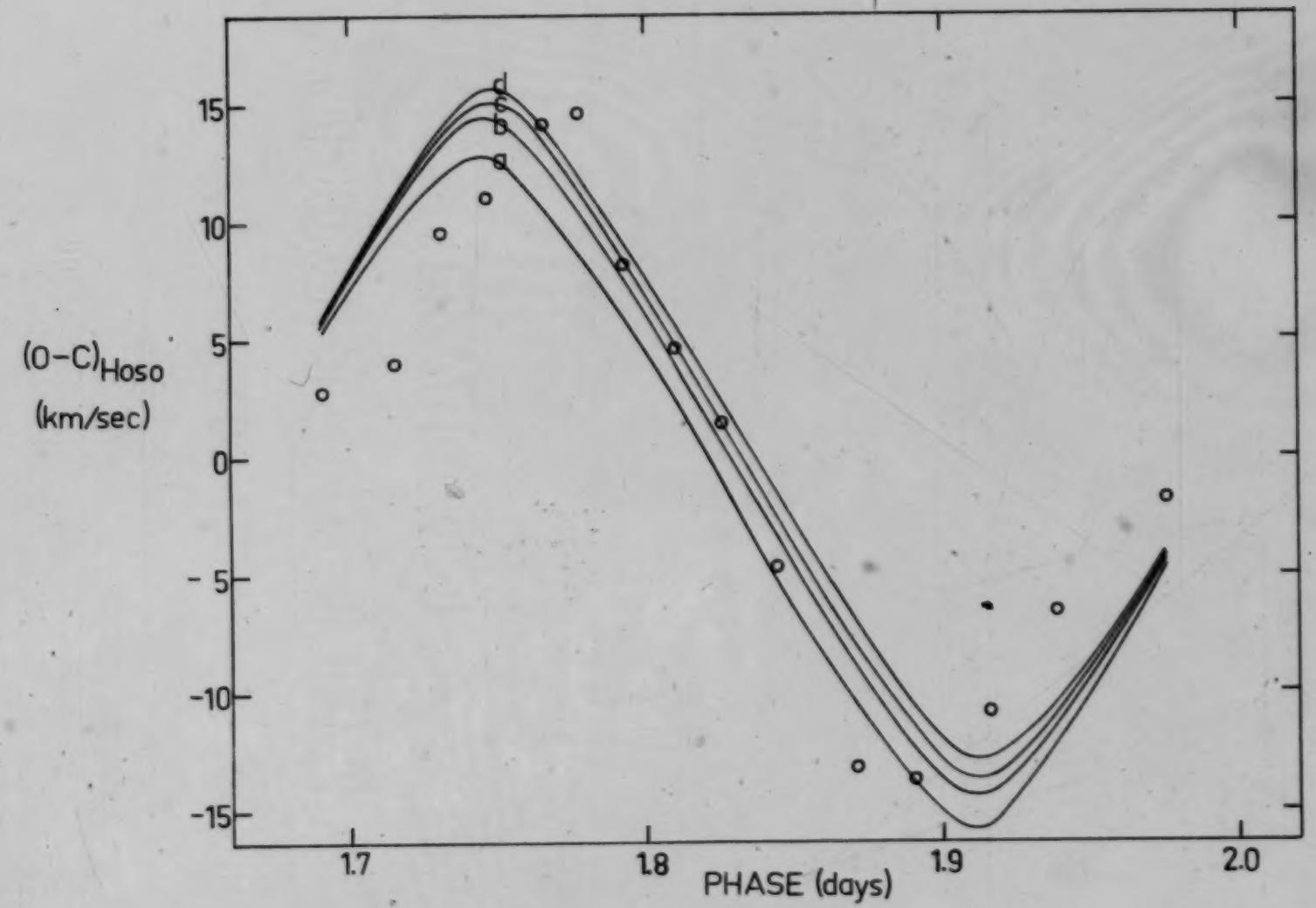
(O-C)Hoso
(km/sec)
15
10
5
0
- 5
-10
-15
1.7
1.8
1.9
2.0
PHASE (days)
d
c
b
a

system does not rotate in synchronism, and so the stars should rotate like single stars, thus supporting the value for V_e obtained for DE Dra.

CHAPTER V

CONCLUDING REMARKS

Thus far, this paper has been concerned with the physical parameters of the spectroscopic binary system DE Dra which can be obtained from the radial velocity measurements of spectrograms, as well as information on the individual components deduced by combining the spectroscopic results with some preliminary photometric data. Many of the results had to be calculated using assumed values for a normal B9V star, and so are only approximate. However they do serve to support some general theories concerning this class of early-type star and in that respect even the rough calculations serve a useful purpose.

As with all scientific research, though, there are many areas which require further investigation in order to build up a complete and firmer knowledge of this system. In the area of spectroscopic studies the fairly detailed analysis presented here has dealt only with the velocity curve of the primary, although the number and quality of the plates has established this very reliably. High dispersion spectrograms in the red or infrared taken near the extremes of the velocity curve (that is, at quadratures) may allow the secondary's spectrum to be seen and thus allow its velocity

curve to be calculated. With velocity curves from both components, certain orbital elements (a, i) can be calculated and compared with those from photometric data.

Some recent higher dispersion plates taken during eclipse before and after conjunction do show evidence of double lines. However this effect is thought to be due to the differential rotational velocity of the visible limbs: the lines are double because although part of the centre of the star is obscured, the limbs which are approaching or receding are still visible. A measurement of the splitting could serve as a means of calculating the absolute rotational velocity since there would be no overall blending from the whole star. The line shifts are due to each limb alone. However, higher resolution is needed before any reliable measurements of the separation can be made. It appears as well that this may be the first system in which this aspect of the separation of different rotation velocities at the limbs has been seen and recognized.

The photometric results for DE Dra are preliminary only. A more detailed analysis with data covering more than one eclipse would yield better values of the inclination, the radii, and the limb-darkening. In particular, if the light curve is observed in more than one effective wavelength the co-efficient of limb-darkening can be more accurately determined. This results from the fact that darkening not only decreases the brightness from centre to limb, but also causes the limb to be redder than the centre. Thus during

an eclipse the colour index of the darkened star should show a gradual change. It should be noted here that any reflection effect in the system (which has not been considered in this paper) will tend to exaggerate the limb-darkening.

Due to the great difference in magnitudes and sizes of the two components, it is not likely that reflection or tidal distortion are important effects for the primary. However the following facts could be kept in mind. The reflection effect shifts the apparent centre of light of each component in the direction of the centre of mass of the system. The effect vanishes at conjunction and is a maximum at quadratures. If not corrected for, this could diminish the true amplitudes, K, of the velocity curves and lead to an underestimate of the true masses and dimensions of the stars. Tidal distortion also affects K and reinforces the reflection effect if $i < 63\overset{\circ}{.}4$ but counteracts it if $i > 63\overset{\circ}{.}4$. Also ellipticity (of stellar shape) and reflection will cause the radial velocity curves to be asymmetric, producing a spurious orbital eccentricity.

An error in the limb-darkening will affect the analysis of the rotation effect. As well, the discrepancy between the calculated curves and the normal points show that for a complete picture, effects other than just limb-darkening must be included. These encompass gravity-darkening, since to every degree of limb-darkening there corresponds a certain amount of gravity-darkening. Centrifugal and tidal forces cause stars to deviate from spheres (an assump-

tion in Chapter IV) and have non-uniform surface brightness. This is due to the fact that limb-darkening makes brightest the parts of the surface nearest the observer, while gravity-darkening makes brightest those nearest the star's centre. In general, on a distorted star the point closest to the observer is not the geometric centre of its apparent disc. In connection with this, gravity-darkening at the tidal bulge, which usually lags behind, can cause the times of spectroscopic conjunction to precede mid-eclipse times, of which there is some evidence in the observations of DE Dra. The variation of angular velocity from pole to equator (in Chapter IV ω was assumed constant) should also be included in the rotation effect analysis. The theory and equations needed for all these are available, and it remains to combine and apply them to DE Dra to obtain a more precise picture of its rotation.

In addition to velocity measurements, analyses of observations of stellar radiation with high-dispersion spectrograms can lead to a knowledge of the conditions (pressure, temperature, chemical composition) in the stellar atmosphere. The available spectrograms also have an intensity calibration spectrum, so measurements can be made which would give line profiles and equivalent widths. The spectrum is scanned with a microphotometer to obtain a density versus wavelength tracing. This is converted into an intensity scale through the intensity calibration spectrum on the plate. The observations are expressed relative to an adopted datum

line called the continuum of the star, which for early-type stars with few strong lines and many weak, shallow ones, is quite easy to define. This represents the intensity distribution of a stellar atmosphere at the same temperature and pressure as the real one, but without any line absorption just absorption in the continuum. The continua observations can be compared directly to continuous fluxes predicted by models to determine a model T_{eff}. It should be noted that any analysis must use rectified intensity tracings, i.e. corrected for distortions due to interstellar matter, Earth's atmosphere, and instrumental broadening. Line profiles are drawn from the rectified tracings and the area of the profile determined, which will yield the equivalent width of the line. The equivalent width of a line increases with increasing element abundance and its distribution among the various states of ionisation and excitation. The shape of the curve of growth changes with atmospheric temperature and pressure. From the spectrum then a set of parameters for the observed curve of growth can be converted through well-investigated formulae into information about atmospheric temperature, pressure, state of atmospheric motion, and element abundance.

Alternately, the observed line profiles and equivalent widths can be compared with those predicted by model atmospheres which are characterised by the parameters T_{eff}, surface gravity g, and chemical composition. In early-type stars the strengths of the Balmer lines are both temperature

and pressure dependent: the outer wing shape is determined by the density of the ions, the inner portion reflects the temperature structure. Thus equivalent widths (element abundances) can be estimated by comparing the observed curve with a set of theoretical profiles having the same shape but different areas. A value for T_{eff} is obtained by comparing the observed Balmer jump with that predicted by models. Also if T_{eff} is correct, the relative strengths of the lines for different stages of ionisation of one element should yield the same element abundance. A knowledge of the element abundances in the atmospheres of normal, main sequence, early-type stars is important because they are among the youngest objects in the HR diagram (about 10^6 to 10^8 years old). Their surface compositions can thus provide information about the present chemical composition of the interstellar matter they were formed from, and a comparison with older objects (the Sun, for example, is about 4.5×10^9 years old) could allow a calculation of the rate of enhancement of interstellar matter with heavier material.

As a side effect of obtaining line profiles and widths from the spectra of DE Dra, an independent determination can be made of the rotational velocity, which would prove interesting. Axial rotation shifts the cores of the spectral lines, but also widens the line profiles. The profiles are asymmetric while the star is being eclipsed, and an analysis of the extent and form of the line asymmetry can give a value for the rotational velocity (and also the geo-

metry of the eclipse itself).

Although the spectroscopic analysis of the primary component of DE Dra is fairly complete, it is evident that much more information can be obtained, not only from further investigations on present spectral data but also from investigations in other observational and theoretical areas. It is hoped that such information as presented here will aid and stimulate further research on this system.

SELECTED BIBLIOGRAPHY

Aitken, R.G. 1964, The Binary Stars. New York: Dover Publications, Inc.

Allen, C.W. 1973, Astrophysical Quantities, 3rd ed. London: Athlone Press.

Batten, A.H. 1961, J. Roy. Astron. Soc. Can. 55, 120.

————. 1973, Binary and Multiple Systems of Stars. Oxford: Pergammon Press.

————. 1976, Publ. Dominion Astrophys. Obs. 14, No. 17.

Chandrasekhar, S. and Münch, G. 1950, Astrophys J. 111, 142.

Crawford, D.L. 1975, Publ. Astron. Soc. Pac. 87, 481.

————. 1978, Astron. J. 83, 48.

Crawford, D.L., Barnes, J.V., Golson J.C., and Hube, D.P. 1973, Astron. J. 78, 738.

Forbes, C. 1911, M.N. 71, 578.

Fuertig, W. 1975, Info. Bull. Var. Stars No. 1071.

Fuertig, W. and Mueninger, L. 1976, Info. Bull. Var. Stars No. 1104.

Golay, M. 1972, Vistas in Astronomy 14 (ed. A. Beer), p. 13. Oxford: Pergammon Press.

————. 1974, Introduction to Astronomical Photometry. Dordrecht, Holland: D. Reidel Publishing Company.

Goodricke, J. 1783, Phil. Trans. Roy. Soc. 73, 474.

Hack, M. and Struve, O. 1969, Stellar Spectroscopy, chap. 3. Trieste: Osservatorio Astronomico.

Hardorp, J. and Strittmatter, P.A. 1968, Astrophys. J. 151, 1057.

Harris, D.L. 1963, Stars and Stellar Systems 3 (ed. K. Aa. Strand), p. 263. Chicago: University of Chicago Press.

Harris, D.L., Strand, K. Aa., and Worley, C.E. 1963, Stars and Stellar Systems 3 (ed. K. Aa. Strand), p. 273. Chicago: University of Chicago Press.

Heintze, J.R.W. 1973, IAU Symp. No. 54 (eds. B. Hauck and B.E. Westerlund), p. 231. Dordrecht, Holland: D. Reidel Publishing Company.

Hellerich, J. 1922, Astron. Nachr. 216, 277.

———. 1924, Astron. Nachr. 223, 369.

Herschel, W. 1802, Phil. Trans. Roy. Soc. for 1802, p. 477.

———. 1803, Phil. Trans. Roy. Soc. for 1803, p. 339.

Holt, J.R. 1893, Astron. and Astrophys. 12, 646.

Hosokawa, Y. 1953, Publ. Astron. Soc. Japan 5, 88.

Hube, D.P. 1973, J. Roy. Astron. Soc. Can. 67, 161.

———. 1976, Info. Bull. Var. Stars No. 1123.

Jaschek, C. 1970, Stellar Rotation (ed. A. Slettebak), p. 219. New York: Gordon and Breach Science Publishers, Inc.

Kitamura, M. 1953, Publ. Astron. Soc. Japan 5, 114.

———. 1965, Advan. Astron. Astrophys. 3, 27.

Kopal, Z. 1942a, Proc. Amer. Phil. Soc. 85, 399.

———. 1942b, Proc. Nat. Acad. Sci. 28, 133.

———. 1945, Proc. Amer. Phil. Soc. 89, 517.

———. 1947, Harvard Circ. No. 450.

———. 1948, J. on Math. Tables and Other Aids to Computation 3, 191.

———. 1955, Ann. Astrophys. 18, 379.

———. 1959, Close Binary Systems. New York: Wiley & Sons Inc.

Kraft, R.P. 1970, Spectroscopic Astrophysics (ed. G.H. Herbig), p. 385. Berkeley: University of California Press.

Lehmann-Filhés, R. 1894, Astron. Nachr. 136, 16.

McLaughlin, D.B. 1924, Astrophys. J. 60, 22.

McLaughlin, D.B. 1934a, Publ. Obs. Univ. Mich. 5, No. 7.

————. 1934b, Publ. Obs. Univ. Mich. 6, No. 2.

McNamara, D.H. 1966, IAU Symp. No. 24 (eds. K. Loden, L.O. Loden, and U. Sinnerstad), p. 190. London: Academic Press.

Nariai, K. 1971, Publ. Astron. Soc. Japan 23, 529.

Petrie, R.M. 1938, Publ. Dominion Astrophys. Obs. 7, 133.

————. 1939, Publ. Dominion Astrophys. Obs. 7, 205.

————. 1950, Publ. Dominion Astrophys. Obs. 8, 319; 341.

————. 1962, Stars and Stellar Systems 2 (ed. W.A. Hiltner), p. 560. Chicago: University of Chicago Press.

Plaskett, J.S. and Young, R.K. 1919, J. Roy. Astron. Soc. Can. 13, 59.

Plaut, L. 1959, Publ. Astron. Soc. Pac. 71, 167.

Plavec, M. 1970, Stellar Rotation (ed. A. Slettebak), p. 133. New York: Gordon and Breach Science Publishers, Inc.

Rossiter, R.A. 1924, Astrophys J. 60, 15.

Roxburgh, I. and Strittmatter, P.A. 1965, Zs. f. Astrophys. 63, 15.

Schlesinger, F. 1908, Publ. Allegheny Obs. 1, 33.

————. 1909, Publ. Allegheny Obs. 1, 123.

Slettebak, A. 1966, Astrophys. J. 145, 126.

Sterne, T.E. 1941, Proc. Nat. Acad. Sci. 27, 175.

Strittmatter, P.A. and Sargent, W.L. 1966, Astrophys. J. 145, 130.

Struve, O. 1950, Stellar Evolution, pp. 125-133. Princeton: Princeton University Press.

Tanner, R.W. 1948, J. Roy. Astron. Soc. Can. 42, 177

Thompson, A.J. 1921, Tracts for Computers No. 5. Cambridge: Cambridge University Press.

Tsesevich [Zessewitch], V.P. 1973, Eclipsing Variable Stars (ed. V.P. Tsesevich), chap. 2. New York: Wiley & Sons Inc.

Underhill, A. 1966, The Early Type Stars. Dordrecht, Holland: D. Reidel Publishing Company.

Vogel, H.C. 1890, Astron. Nachr. 123, 289.

Willmarth, D.W. 1976, Publ. Astron. Soc. Pac. 88, 86.

Zessewitch [Tsesevich], V.P. 1939, Bull. Astron. Inst. Leningrad No. 45.

_____: 1940, Bull. Astron. Inst. Leningrad No. 50.

APPENDIX A

OBSERVATIONAL DATA

The observations presented here include both non-eclipse and eclipse data from the DDO and the DAO. Observations numbered 1 to 19 inclusive are from DDO plates, of which numbers 18 and 19 are eclipse data. The remaining observations from numbers 20 to 105 are from DAO plates, and of these the last 51, from numbers 55 to 105 inclusive, are eclipse data.

The column headings denote the following quantities:

V: the observed heliocentric radial velocity in km/s

TIME: the phase of the observation in days

O-C: the observed velocity minus the calculated velocity in km/s

MEAN A: the mean anomaly M, in radians, = $\frac{2\pi}{P}(t-T)$

ECC A: the eccentric anomaly E, inradians, determined from the formula M = E-esinE

TRUE A: the true anomaly ν, in radians, calculated from $\tan \frac{\nu}{2} = \frac{1+e}{1-e} \tan \frac{E}{2}$

U: the argument of the latitude $u = \nu+\omega$, in rad

C: the velocity in km/s calculated from the orbital elements, = γ + Kecosω + Kcosu

I	JULIAN DAY	V	TIME	O-C	MEAN A	ECC A	TRUE A	U	C
1	2440802.755	39.1	0.870	-3.4	1.031	1.053	1.075	6.719	42.5
2	2440809.780	-44.4	2.596	-1.3	3.079	3.081	3.082	8.726	-43.1
3	2441141.721	43.8	0.755	-1.3	0.895	0.916	0.936	6.580	45.1
4	2441147.689	16.3	1.425	-3.0	1.690	1.715	1.740	7.384	19.3
5	2441147.832	10.1	1.568	-1.3	1.859	1.884	1.908	7.551	11.4
6	2441148.634	-31.6	2.370	1.9	2.810	2.819	2.827	8.470	-33.5
7	2441148.827	-46.9	2.563	-5.1	3.039	3.042	3.044	8.688	-41.8
8	2441159.655	-50.0	2.795	-0.6	3.314	3.310	-2.977	2.666	-49.4
9	2441159.846	-53.5	2.986	-0.1	3.541	3.531	-2.762	2.882	-53.4
10	2441160.627	-47.1	3.767	-2.0	4.467	4.442	-1.865	3.779	-45.1
11	2441160.848	-35.5	3.988	0.3	4.729	4.704	-1.605	4.039	-35.8
12	2441457.793	-21.0	4.237	1.7	5.025	5.001	-1.307	4.337	-22.7
13	2441458.752	32.6	5.196	-0.4	6.162	6.159	-0.127	5.517	33.0
14	2441462.778	-36.5	3.924	2.3	4.654	4.628	-1.680	3.964	-38.8
15	2441463.771	22.5	4.917	3.8	5.831	5.820	-0.475	5.169	18.7
16	2441463.826	17.4	4.972	-4.4	5.896	5.887	-0.406	5.237	21.8
17	2443298.800	19.5	1.494	4.0	1.772	1.796	1.821	7.465	15.5
18	2440803.681	5.2	1.796	7.1	2.129	2.151	2.172	7.816	-1.9
19	2440803.754	-25.6	1.869	-19.4	2.216	2.236	2.256	7.900	-6.2
20	2442955.747	-50.7	2.820	-0.6	3.344	3.339	-2.949	2.695	-50.1
21	2442955.827	-52.1	2.900	-0.2	3.439	3.431	-2.859	2.785	-51.9
22	2442975.742	5.1	1.622	-3.2	1.924	1.947	1.971	7.615	8.3
23	2442975.800	2.4	1.680	-2.5	1.992	2.015	2.038	7.682	4.9
24	2442975.816	2.0	1.696	-1.9	2.011	2.034	2.057	7.701	3.9
25	2442976.799	-47.0	2.679	-1.0	3.177	3.176	-3.108	2.536	-46.0
26	2442992.779	-48.4	2.765	0.2	3.279	3.275	-3.011	2.633	-48.6
27	2442992.936	-49.8	2.922	2.5	3.465	3.457	-2.834	2.810	-52.3
28	2443053.723	39.4	0.131	-2.2	0.155	0.159	0.163	5.807	41.6
29	2443081.594	15.6	1.511	1.0	1.792	1.817	1.842	7.485	14.6
30	2443081.625	13.1	1.542	0.3	1.829	1.853	1.878	7.522	12.8
31	2443081.654	10.1	1.571	-1.1	1.863	1.888	1.912	7.556	11.2

I	JULIAN DAY	V	TIME	O-C	MEAN A	ECC A	TRUE A	U	C
32	2443081.693	8.5	1.610	-0.4	1.910	1.933	1.957	7.601	8.9
33	2443102.681	24.7	1.406	4.4	1.667	1.692	1.718	7.361	20.3
34	2443104.697	-51.8	3.422	1.9	4.058	4.038	-2.265	3.379	-53.7
35	2443262.951	-45.2	2.732	2.5	3.240	3.237	-3.048	2.596	-47.7
36	2443263.934	-50.4	3.715	-3.6	4.405	4.381	-1.926	3.718	-46.8
37	2443264.795	-10.2	4.576	-8.1	5.427	5.407	-0.896	4.748	-2.1
38	2443264.811	-0.4	4.592	0.7	5.446	5.426	-0.876	4.768	-1.1
39	2443264.848	2.8	4.629	1.5	5.489	5.471	-0.831	4.813	1.3
40	2443264.871	2.7	4.652	0.0	5.517	5.499	-0.803	4.841	2.7
41	2443264.884	0.7	4.665	-2.8	5.532	5.514	-0.787	4.857	3.5
42	2443264.905	11.2	4.686	6.4	5.557	5.540	-0.761	4.883	4.8
43	2443264.923	3.2	4.704	-2.7	5.578	5.562	-0.739	4.905	5.9
44	2443264.965	9.8	4.746	1.3	5.628	5.612	-0.687	4.957	8.5
45	2443264.984	12.1	4.765	2.4	5.651	5.635	-0.663	4.981	9.7
46	2443366.827	51.5	0.645	4.8	0.765	0.783	0.801	6.445	46.7
47	2443333.830	6.8	4.735	-1.1	5.615	5.599	-0.700	4.944	7.9
48	2443367.777	12.1	1.595	2.3	1.892	1.916	1.939	7.583	9.8
49	2443330.736	5.4	1.641	-1.8	1.946	1.970	1.993	7.637	7.2
50	2443264.984	12.6	4.765	2.9	5.651	5.635	-0.663	4.981	9.7
51	2443331.909	-49.9	2.814	0.0	3.337	3.332	-2.955	2.688	-49.9
52	2443331.756	-45.7	2.661	-0.3	3.156	3.155	-3.128	2.516	-45.4
53	2443330.751	10.6	1.656	4.3	1.964	1.987	2.010	7.654	6.3
54	2443368.800	-40.8	2.618	3.1	3.105	3.106	3.107	8.751	-43.9
55	2442954.731	-0.5	1.804	1.9	2.139	2.160	2.181	7.825	-2.4
56	2442954.768	-4.5	1.841	0.1	2.183	2.203	2.224	7.867	-4.6
57	2442954.806	-20.5	1.879	-13.7	2.228	2.248	2.267	7.911	-6.8
58	2442954.840	-19.3	1.913	-10.5	2.268	2.287	2.306	7.950	-8.8
59	2442954.914	-12.5	1.987	0.6	2.356	2.374	2.391	8.035	-13.1
60	2442975.838	3.9	1.718	1.3	2.037	2.060	2.082	7.726	2.6
61	2442975.861	11.2	1.741	9.9	2.065	2.087	2.109	7.753	1.3
62	2442975.893	8.7	1.773	9.3	2.103	2.124	2.146	7.790	-0.6

I	JULIAN DAY	V	TIME	O-C	MEAN A	ECC A	TRUE A	U	C
63	2442975.908	4.1	1.788	5.6	2.120	2.142	2.163	7.807	-1.5
64	2442975.929	3.2	1.809	5.9	2.145	2.166	2.187	7.831	-2.7
65	2442975.948	-4.9	1.828	-1.1	2.168	2.189	2.209	7.853	-3.8
66	2442975.969	-13.5	1.849	-8.4	2.193	2.213	2.233	7.877	-5.1
67	2442991.775	12.2	1.761	12.1	2.088	2.110	2.131	7.775	0.1
68	2442991.780	12.2	1.766	12.4	2.094	2.116	2.137	7.781	-0.2
69	2442991.785	15.3	1.771	15.7	2.100	2.121	2.143	7.787	-0.4
70	2442991.790	11.2	1.776	11.9	2.106	2.127	2.149	7.793	-0.7
71	2442991.795	15.6	1.781	16.6	2.112	2.133	2.154	7.798	-1.0
72	2442991.802	5.7	1.788	7.2	2.120	2.141	2.163	7.806	-1.5
73	2442991.822	3.2	1.808	5.8	2.144	2.165	2.186	7.829	-2.6
74	2442991.829	0.9	1.815	3.9	2.152	2.173	2.194	7.838	-3.0
75	2442991.835	-5.4	1.821	-2.0	2.159	2.180	2.201	7.844	-3.4
76	2442991.843	-3.5	1.829	0.4	2.169	2.189	2.210	7.854	-3.9
77	2442991.849	-6.8	1.835	-2.6	2.176	2.196	2.217	7.861	-4.2
78	2442991.855	-7.5	1.841	-2.9	2.183	2.203	2.224	7.867	-4.6
79	2442991.861	-8.9	1.847	-4.0	2.190	2.210	2.231	7.874	-4.9
80	2442991.866	-15.3	1.852	-10.1	2.196	2.216	2.236	7.880	-5.2
81	2442991.882	-18.8	1.868	-12.6	2.215	2.235	2.255	7.899	-6.2
82	2442991.901	-24.3	1.887	-17.0	2.237	2.257	2.276	7.920	-7.3
83	2442991.907	-17.9	1.893	-10.3	2.244	2.264	2.283	7.927	-7.6
84	2442991.930	-20.2	1.916	-11.2	2.272	2.291	2.310	7.954	-9.0
85	2442991.933	-19.9	1.919	-10.7	2.275	2.294	2.313	7.957	-9.2
86	2442991.948	-20.7	1.934	-10.7	2.293	2.312	2.330	7.974	-10.0
87	2442991.952	-18.7	1.938	-8.4	2.298	2.316	2.335	7.979	-10.3
88	2442991.959	-11.5	1.945	-0.8	2.306	2.325	2.343	7.987	-10.7
89	2442991.980	-13.5	1.966	-1.6	2.331	2.349	2.367	8.011	-11.9
90	2442991.985	-16.6	1.971	-4.4	2.337	2.355	2.373	8.017	-12.2
91	2443261.947	13.3	1.728	11.2	2.049	2.071	2.093	7.737	2.1
92	2443367.977	9.0	1.795	10.9	2.129	2.150	2.171	7.815	-1.9
93	2443368.006	6.0	1.824	9.6	2.163	2.184	2.205	7.849	-3.6

I	JULIAN DAY	V	TIME	O-C	MEAN A	ECC A	TRUE A	U	C
94	2443367.931	12.4	1.749	11.6	2.074	2.096	2.118	7.762	0.8
95	2443330.861	16.2	1.766	16.4	2.094	2.116	2.138	7.782	-0.2
96	2443330.924	-3.4	1.829	0.5	2.169	2.190	2.210	7.854	-3.9
97	2443330.845	12.5	1.750	11.7	2.075	2.097	2.119	7.763	0.8
98	2443330.878	19.4	1.783	20.6	2.115	2.136	2.157	7.801	-1.2
99	2443330.830	9.4	1.735	7.8	2.058	2.080	2.102	7.746	1.6
100	2443330.962	-12.7	1.867	-6.6	2.214	2.234	2.254	7.898	-6.1
101	2443330.909	2.9	1.814	5.9	2.151	2.172	2.193	7.837	-3.0
102	2443330.894	8.2	1.799	10.3	2.134	2.155	2.176	7.820	-2.1
103	2443330.794	6.5	1.699	2.7	2.015	2.038	2.060	7.704	3.8
104	2443330.810	9.4	1.715	6.6	2.034	2.056	2.079	7.723	2.8
105	2443330.778	7.5	1.683	2.8	1.996	2.019	2.042	7.686	4.7

APPENDIX B

CALCULATION OF PHYSICAL PARAMETERS

Colour and magnitude

The description of the uvbyβ system given by Crawford (1975) contains the following definitions of the parameters:

$$E(c_1) = 0.20E(b-y)$$

$$E(u-b) = 1.5E(b-y)$$

$$m_1 = (v-b) - (b-y)$$

$$c_1 = (u-v) - (v-b)$$

$$(u-b) = c_1 + 2m_1 + 2(b-y)$$

$$(u-b)_o = 1.13(u-b) - 1.70(b-y) - 0.186$$

The photometry of Crawford et al (1973) resulted in values of the indices for DE Dra of:

$$\beta = 2.824$$

$$b-y = -0.017$$

$$m_1 = 0.123$$

$$c_1 = 0.873$$

These values are substituted into the above equations to yield:

$$(u-b) = 1.085$$

$$(u-b)_o = 1.069$$

Then $E(u-b) = 0.016$ $[= (u-b) - (u-b)_o]$

and $E(c_1) = 0.002$

The subscript 'o' and the letter E( ) refer to the unreddened index and the colour excess respectively. Thus the unreddened parameter c_o can be found. This allows us to calculate the absolute visual magnitude using the recent calibration of the uvbyβ system performed by Crawford (1978). He gives a table relating the c_o value to a value of β(ZAMS) (i.e. the strength of the Hβ line for unevolved B-type stars), which is then related to a value for the M_v(ZAMS). However, due to evolutionary effects, the value of β(observed) will not be the same as the tabulated β(ZAMS) for that value of c_o. Therefore a correction must be made to the M_v(ZAMS) to obtain the correct M_v. The above calculations for DE Dra procede as follows:

$$c_o = c_1 - E(c_1) = 0.871 \quad \text{(from previous page)}$$

$$\beta(\text{ZAMS}) = 2.857 \quad \text{(from Crawford 1978)}$$

$$M_v(\text{ZAMS}) = 1.08$$

$$\Delta\beta = \beta(\text{ZAMS}) - \beta(\text{observed}) = 0.033$$

$$\Delta M_v = 10\Delta\beta = 0.33$$

Then

$$M_v = M_v(\text{ZAMS}) - \Delta M_v = 0.75$$

This value agrees well with that expected of a B9V star. Crawford also gave a relation between the uvbyβ system and the UBV system:

$$(U-B)_o = -0.94 + 0.86c_o$$

This gives a value for DE Dra of $(U-B)_o = -0.19$ which also agrees well with the value expected for a B9V star in the MK system.

Mass

Different values for the mass have been calculated from the various formulae given by five authors. The final value adopted in chapter III is an average of these.

1. Allen (1973)

(for the value of M_{bol} see the sections Bolometric correction and Bolometric magnitude)

$$M_{bol} = 4.75 - 2.5\log \frac{L}{L_\odot}$$

$$\log \frac{L}{L_\odot} = 3.45\log \frac{M}{M_\odot}$$

Then $$M = 3.38M_\odot$$

2. Batten (1968)

$$M_V = -5.559\log(M) + 2.485$$

$$M = 2.05M_\odot$$

3. Petrie (1950)

$$\log(M) = 0.548 - 0.144M_c + 0.002M_c^2$$

$$M_c = M_{bol} + 2\log \frac{T_e}{5200} = 0.864$$

$$M = 2.66M_\odot$$

4. Harris, Strand, and Worley (1963)

$$M_{bol} = 4.6 - 10.0\log(\ ) \quad \text{for } M_{bol} \ +7.5$$

$$M = 2.76M_\odot$$

5. Kopal (1959)

$$\log(M) = 0.45 - 0.143M_{bol} \quad \text{for } M > 2M_{\odot}$$

$$M = 2.65M_{\odot}$$

The average value of the five values above is then

$$M_{av} = 2.70M_{\odot}$$

Distance

The value of V, the apparent visual magnitude uncorrected for reddening, was published by Crawford et al (1973) for DE Dra as V = +5.72. The standard relationship for interstellar absorption was used, as well as the values from the photometry for the colour excesses.

$$\left.\begin{aligned} E(b-y) &= 0.74E(B-V) \\ E(u-b) &= 1.5E(b-y) \end{aligned}\right\} \quad \text{(Crawford 1975)}$$

$$A_V = 3.3E(B-V) = \frac{3.3}{.74}\,\frac{1}{1.5}\,E(u-b)$$

$$= +0.048$$

$$V_o = V - 0.048$$

$$= +5.67$$

Then $$V_o - M_V = 5\log(d) - 5 = +4.92$$

$$d = 96.4 \text{ parsecs}$$

Effective temperature

The effective temperature of 11,300°K is an average value of three quantities obtained from formulae given by Heintze (1973) relating $(U-B)_o$ to $\theta_{eff} = \frac{5040}{T_{eff}}$.

Bolometric correction

The bolometric correction was calculated using the formula in Allen (1973):

$$-B.C. = -42.54 + \log T_{eff} + \frac{29000}{T_{eff}}$$

$$B.C. = -0^{m}.56$$

Bolometric magnitude

From the above B.C. the value of M_{bol} is:

$$M_{bol} = M_{v} + B.C.$$

$$= +0^{m}.19$$

Radius

An average value of the radius was calculated from two formulae relating M_{bol} and R:

1. Allen (1973)

$$\log \frac{R}{R_{\odot}} = \frac{1}{5} [\ 42.36 - 10 \log T_{eff} - M_{bol}]$$

$$R = 2.13\ R_{\odot}$$

2. Kopal (1959)

$$0.45 - 0.143 M_{bol} = 1.57 \log R - 0.15 \quad \text{for } M > 2M_{\odot}$$

$$R = 2.32\ R_{\odot}$$

This gives a value for R of the primary of:

$$R_{av} = 2.2\ R_{\odot} = R_{1}$$

and from the photometric value k = 0.35:

$$R_{2} = 0.8\ R_{\odot}$$

However because of the great uncertainty in the value of M_{bol} it was decided to use the spectroscopic value of the

mass function f(M), the calculated mass M_1, and the photometric value of i to calculate values for a_1, M_2, R_1, and R_2. From $M_1 = 2.7\ M_\odot$ and $i \simeq 87°$, $r_1 = 0.157$, $r_2 = 0.055$:

$$f(M) = \frac{M_2^3 \sin^3 i}{(M_1+M_2)^2} = 0.074$$

$$M_2 = 1.0\ M_\odot$$

$$a_1 \sin i = 3.73 \times 10^6$$

$$a_1 = 3.74 \times 10^6 \text{ km}$$

$$a_2 = \frac{M_1}{M_2} a_1 = 9.99 \times 10^6 \text{ km}$$

$$a = a_1 + a_2 = 13.7 \times 10^6 \text{ km}$$

$$R_1 = a r_1 = 3.1\ R_\odot$$

$$R_2 = a r_2 = 1.1\ R_\odot$$